https://doi.org/10.1093/plphys/kiac486 PLANT PHYSIOLOGY 2023: 191: 643–659

Plant Physiology®

Research Article

A stress-inducible protein regulates drought tolerance and flowering time in *Brachypodium* and Arabidopsis

Sheng Ying [1,2,3,*] **Wolf-Rüdiger Scheible** [3] **and Peter Knut Lundquist** [1,2,*]

1 Department of Biochemistry and Molecular Biology, Michigan State University, East Lansing, Michigan 48824, USA
2 Plant Resilience Institute, Michigan State University, East Lansing, Michigan 48824, USA
3 Noble Research Institute LLC, Ardmore, Oklahoma 73401, USA

*Authors for correspondence: pklundqu@msu.edu (P.K.L.) and yingshen@msu.edu (S.Y.)
Conceptualization, methodology, investigation, writing of the original draft, writing and reviewing was done by S.Y. Conceptualization, methodology, writing and reviewing and editing, supervision, and funding acquisition was done by W.-R.S. and P.K.L.
The author responsible for distribution of materials integral to the findings presented in this article in accordance with the policy described in the Instructions for Authors (https://academic.oup.com/plphys/pages/general-instructions) is Peter K. Lundquist (pklundqu@msu.edu).

Abstract

To cope with environmental stresses and ensure maximal reproductive success, plants have developed strategies to adjust the timing of their transition to reproductive growth. This has a substantial impact on the stress resilience of crops and ultimately on agricultural productivity. Here, we report a previously uncharacterized, plant-specific gene family designated as Regulator of Flowering and Stress (RFS). Overexpression of the *BdRFS* gene in *Brachypodium distachyon* delayed flowering, increased biomass accumulation, and promoted drought tolerance, whereas clustered regularly interspaced short palindromic repeats/CRISPR-associated protein 9 (CRISPR/Cas9)-mediated knockout mutants exhibited opposite phenotypes. A double T-DNA insertional mutant in the two Arabidopsis (*Arabidopsis thaliana*) homologs replicated the effects on flowering and water deprivation seen in the *B. distachyon* CRISPR knockout lines, highlighting the functional conservation of the family between monocots and dicots. Lipid analysis of *B. distachyon* and Arabidopsis revealed that digalactosyldiacylglycerol (DGDG) and phosphatidylcholine (PC) contents were significantly, and reciprocally, altered in overexpressor and knockout mutants. Importantly, alteration of C16:0-containing PC, a Flowering Locus T-interacting lipid, associated with flowering phenotype, with elevated levels corresponding to earlier flowering. Co-immunoprecipitation analysis suggested that BdRFS interacts with phospholipase Dα1 as well as several other abscisic acid-related proteins. Furthermore, reduction of C18:3 fatty acids in DGDG corresponded with reduced jasmonic acid metabolites in CRISPR mutants. Collectively, we suggest that stress-inducible RFS proteins represent a regulatory component of lipid metabolism that impacts several agronomic traits of biotechnological importance.

Introduction

Terrestrial plants are exposed to a wide range of environmental stresses that severely affect their growth and development. To survive, plants have evolved elaborate mechanisms and complex regulatory networks to cope with these stresses. Such mechanisms often involve remodeling of membrane lipid composition (Liu et al., 2019). While chloroplast membranes are dominated by the galactolipids monogalactosyldiacylglycerol (MGDG) and digalactosyldiacylglycerol (DGDG), biological membranes outside of the chloroplast consist primarily of phospholipids. Under phosphorus (P) deficiency, intracellular phospholipids are rapidly hydrolyzed by various phospholipases to conserve inorganic phosphate (P_i) for other essential processes, and their

Received May 24, 2022. Accepted September 25, 2022. Advance access publication October 20, 2022

Open Access

membrane structural roles are substituted by MGDG and DGDG, or the sulfolipid sulfoquinovosyldiacylglycerol (Nakamura, 2013; Pfaff et al., 2020; Sun et al., 2020; Ali et al., 2022). In P-starved Arabidopsis (*Arabidopsis thaliana*), phospholipase D (PLD) ζ1 and ζ2 hydrolyze phosphatidylcholine (PC) to release P_i and diacylglycerol (DAG), promoting DGDG synthesis (Li et al., 2006). In addition, altering polyunsaturated fatty acid (FA; PUFA) levels of membrane lipids can help plants adapt to environmental stresses through alteration of membrane fluidity and stability. For instance, overexpression of FA desaturases can enhance plant tolerance to numerous abiotic stresses (Yu et al., 2021).

Brachypodium distachyon is a globally distributed C3 temperate grass. Desirable properties such as small genome size, short life cycle, self-fertility, availability of whole-genome sequences, and relative ease of genetic transformation, make *B. distachyon* a powerful resource for fundamental research on small cereal crops such as wheat (*Triticum aestivum*), rye (*Secale cereale*), or barley (*Hordeum vulgare*) (Scholthof et al., 2018; Raissig and Woods, 2022). Hence, *B. distachyon* has been adopted as a model organism for the study of flowering time and adaptive responses to abiotic/biotic stresses or nutrient deficiencies (Priest et al., 2014; Woods et al., 2017; David et al., 2019; Qin et al., 2019).

Flowering time (also known as heading time in grasses) is a critical trait that determines grain yield, biomass production, and reproductive success. To maximize yield, the flowering time of cereals crops has been domesticated according to the specific requirements of the grower and crop species (Cockram et al., 2007). Delayed flowering is generally a desirable trait for biofuel or forage crops, where vegetative biomass is the material of use. In contrast, an early flowering trait is generally desired in cereal crops where a shortened time to harvest can permit additional plantings in a growing season and a reduced threat of biotic and abiotic stresses (Bheemanahalli et al., 2017; Shavrukov et al., 2017). The timing of flowering is regulated through complex systems that have been intensively studied, revealing a number of key floral integrators. Of particular note, Flowering Locus T (FT) plays a conserved and dominant role in determination of plant flowering time by regulating shoot meristematic activity (Jin et al., 2021). FT binds to PC, favoring species with more saturated acyl chains, to promote flowering (Nakamura et al., 2014). The acyl composition of PC oscillates with the diurnal cycle and changes in response to environmental stimuli. FT interacts most effectively with saturated PC species, such as C16:0, that accumulate during the light period. Thus, it was concluded that FT preferentially binds to more saturated PC species to promote flowering time. On the other hand, FT can also interact with negatively charged phosphatidylglycerol (PG, especially 34:4 and 34:3 species) at low ambient temperature (Susila et al., 2021). This interaction inhibits the translocation of FT from companion cells to sieve elements, thereby preventing precocious flowering.

Flowering time is substantially affected by abiotic stresses such as drought or low temperature (Kazan and Lyons, 2015; Cho et al., 2017). During drought stress, plants flower earlier to escape the harsh environments, while nutrient starvation (e.g. nitrogen [N] or P) results in delayed flowering (Kant et al., 2011; Riboni et al., 2013; Lin and Tsay, 2017). In *B. distachyon*, several key regulators of flowering time, such as FT1, FT-Like9, microRNA5200, and Early Flowering 3 have been identified and functionally characterized (Ream et al., 2013; Wu et al., 2013; Qin et al., 2017, 2019; Woods et al., 2019; Bouché et al., 2022). *Brachypodium distachyon* FT1 protein, and its closest paralog FT2, have been shown to regulate flowering time, spikelet development, and fertility (Ream et al., 2013; Lv et al., 2014; Shaw et al., 2019). Ecological studies have shown that due to its low water use efficiency, *B. distachyon* prefers to live in higher, cooler, and wetter locations (i.e. north of 33° latitude) compared to other *Brachypodium* species (Scholthof et al., 2018). Nevertheless, how *B. distachyon* adjusts its habits (e.g. flowering time) to adverse environments is poorly understood.

Here, we investigated members of a conserved, plant-specific gene family that we name the *Regulator of Flowering and Stress* (*RFS*) family. This family encodes proteins of ∼22 kDa, distinguished by a single N-terminal transmembrane helix and a conserved but uncharacterized domain. Transcript levels of several *RFS* genes were strongly affected by environmental stimuli (e.g. P availability, drought, or freezing stress). Overexpression of the *B. distachyon* homolog *BdRFS* (Bd4g31140) not only substantially delayed flowering/heading time but also enhanced biomass accumulation and drought tolerance. Knockout mutants of *RFS* genes in Arabidopsis or *B. distachyon* had early flowering phenotypes and were hypersensitive to water deficit. Thorough lipid analyses of mutants demonstrate that RFS proteins appear to modulate lipid metabolism to impact these agronomic traits. Thus, the *RFS* gene family is identified as a stress-inducible effector of flowering time and drought tolerance.

Results

Conserved *RFS* genes respond to multiple abiotic stresses

The Arabidopsis *RFS* genes, *AtRFS1* (At3g43110) and *AtRFS2* (At5g20790), have been proposed as hallmark genes of the P-limitation response (Bari et al., 2006). Reverse transcription–quantitative PCR (RT–qPCR) assays confirmed the strong induction of both gene transcripts in shoot and root tissue during P-limitation (Figure 1A). Following P re-addition, both transcript levels dropped rapidly within 3 h, indicating a direct response to P-status (Figure 1B). Notably, *AtRFS1* and *AtRFS2* gene transcripts were strongly induced by P-limitation only, but either not at all or much less by sulfur, N, and carbon limitation (Figure 1C). Promoter-β-glucuronidase (GUS) staining assays revealed complementary tissue expression patterns between the two homologs. While staining assays revealed no distinguishable GUS signals in P-replete conditions, under P-stress, *AtRFS1* was expressed

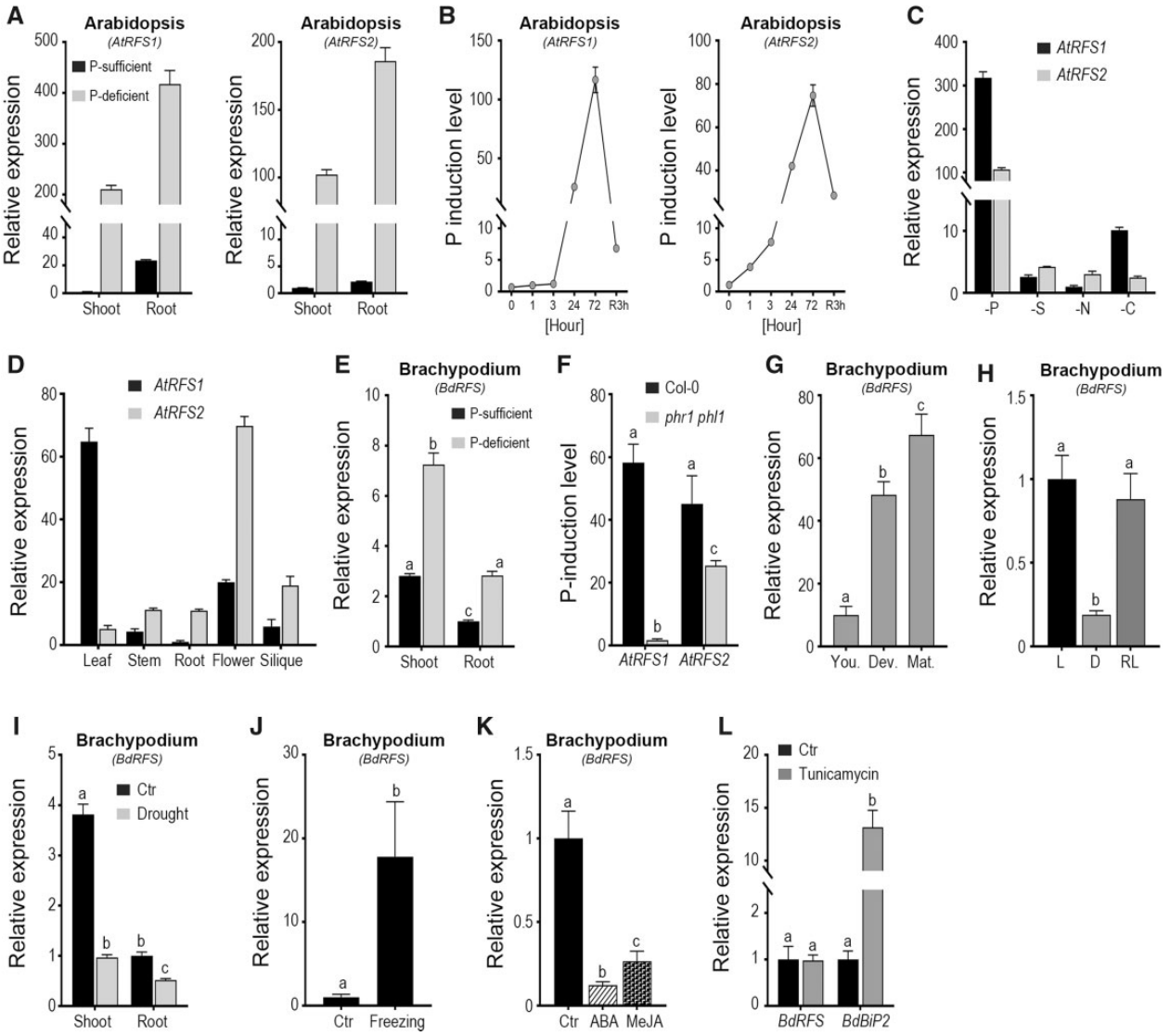

Figure 1 Expression patterns of *RFS* genes in Arabidopsis and *B. distachyon*. A–D, transcript changes of *AtRFS* genes, *AtRFS1* (At3g43110) and *AtRFS2* (At5g20790), in shoot or root under P-deficiency (A), during a P-deprivation and re-addition time course (B), under nitrogen (–N), sulfur (–S), or carbon (–C) deficiency (C), or in different tissues (D). E–L, transcript changes of the *BdRFS* gene (Bd4g31140), under P-stress (E), at different developmental stages of leaves (G), under dark (H), drought (I), freezing (J), ABA, and MeJA (K), or tunicamycin (Tm) (L) treatments. In (B), R3h, 3 h after P-re-addition. In (G), You., young leaves; Dev., developing leaves; Mat., mature leaves. In (H), L., light condition; D., dark condition; RL., restored light condition. (F) P-stress induction level (–P versus +P) of the *AtRFS* genes in wild-type (WT) and *phr1 phl1* double mutant. *Arabidopsis Glyceraldehyde-3-Phosphate Dehydrogenase* (*AtGAPDH*) or *B. distachyon Ubiquitin-conjugating enzyme 18 (BdUBC18)* gene was used as reference housekeeping gene for normalization of reverse transcription quantitative polymerase chain reaction (RT–qPCR) values. The *B. distachyon BdBiP2* gene is used as positive control of Tm treatment (L). The data represent the mean values of three replicates ±1 SD. Statistical significance of differences is tested by one-way analysis of variance (ANOVA) analysis ($P < 0.001$) and is indicated by lower-case letters.

in the leaf apex, root meristem, and root tip, whereas *AtRFS2* was expressed in leaves and primary root but not in the root tip (Supplemental Figure S1). Furthermore, RT–qPCR assays of P-replete Arabidopsis tissue demonstrated that both homologs are expressed at low levels, with *AtRFS1* preferentially expressed in leaves and *AtRFS2* predominant in flowers (Figure 1D). Furthermore, both homologs are strongly expressed in seeds (Supplemental Figure S2).

Orthologs of *RFS* genes were identified in both monocots and eudicots (Supplemental Table S1). Protein sequence alignment revealed a high degree of conservation in the N-terminal transmembrane domain and C-terminus of proteins (Supplemental Figure S3). To better understand their evolutionary relationship, a phylogenetic tree consisting of RFS protein sequences from eight monocots (*B. distachyon*, rice (*Oryza sativa*), maize (*Zea mays*), sorghum (*Sorghum bicolor*), foxtail millet (*Setaria italica*), switchgrass (*Panicum virgatum*), barley, and wheat and three eudicot species (Arabidopsis, *Medicago truncatula*, and soybean [*Glycine max*]) was constructed. While single copies of *RFS* were

identified in monocot genomes, dicots harbored two homologs (or three in the tetraploid soybean). Monocot and dicot RFS proteins were divided into distinct monocot and dicot clades (Supplemental Figure S3A). These results indicate that RFS proteins are conserved throughout the land plant lineage, and that their sequence conservation is largely concordant with the species tree. Comparable to Arabidopsis, the orthologous *RFS* genes in *M. truncatula*, rice, and maize were strongly induced by P-limitation in both root and shoot tissue (Supplemental Figure S4, A and B). In *B. distachyon*, *RFS* genes were also induced although somewhat less than in the other investigated species (Figure 1E).

Phosphate Starvation Response 1 and PHR1-like 1 are critical transcription factors in P-signaling (Rubio et al., 2001; Nilsson et al., 2007; Bustos et al., 2010). During P-limitation, *AtRFS1* and *AtRFS2* transcript levels were clearly reduced in a *phr1 phl1* double mutant (Figure 1F), consistent with a previous report (Castrillo et al., 2017), indicating their transcriptional dependence on PHR1 and PHL1 (Bustos et al., 2010). Similarly, abundance of the rice *OsRFS* gene transcript, LOC_Os09g26670, was dependent on OsPHRs (Supplemental Figure S4C). These results suggest that plant *RFS* genes are integrated within PHR1/PHL1-regulated signaling networks.

Brachypodium distachyon is the model plant of choice for studying the biology of temperate C3 grasses and offers a powerful resource for the improvement of cereal and biofuel crops. Thus, we investigated the expression profiles of the *B. distachyon BdRFS* gene (Bd4g31140) in more detail. Notably, *BdRFS* transcript increased over six-fold during leaf maturation, consistent with public datasets for rice and maize (Figure 1G; Supplemental Figure S5). On the other hand, *BdRFS* transcript was reduced in the dark (Figure 1H). To investigate whether *BdRFS* transcript abundance may be subject to PHR1 TF, we scanned the promoter region (3-kb upstream of start codon) for PHR1 binding sites (P1BS, GNATATNC, where N represents any base). Two P1BS sequences were found at 231- and 491 bp upstream of the start codon. Moreover, cis-regulatory elements (CREs) related to drought stress, low temperature, and abscisic acid (ABA)/methyl jasmonate (MeJA) responses were identified in the *BdRFS* promoter region. Therefore, we hypothesized that *BdRFS* might respond to environmental stimuli and endogenous phytohormones. *BdRFS* transcript abundance was induced during freezing treatment but suppressed during drought or phytohormones (ABA or MeJA) treatments (Figure 1, I–K). P-limitation activates endoplasmic reticulum (ER) stress and then elicits the unfolded protein response (Naumann et al., 2019). We treated 7-day-old *B. distachyon* wild-type (BD21-3) seedlings with tunicamycin (Tm) to stimulate ER stress (Kim et al., 2017). RT–qPCR showed that *BdRFS* transcript abundance was not induced by Tm treatment (Figure 1L). *RFS* genes in other grasses (e.g. rice, barley, and maize) or in Arabidopsis exhibited similar expression patterns to abiotic stresses (drought and freezing) or ABA treatment (Supplemental Figure S4, E–H). Collectively, these findings suggest that plant *RFS* genes are conserved in land plants and respond to various environmental stimuli.

RFS proteins may localize to ER and cytosol

To investigate the subcellular localization of plant RFS proteins, we first searched proteomic databases and subcellular localization prediction tools, namely SUBA4, WoLF P-Sort, TargetP, and the Plant Proteome Database (Horton et al., 2007; Sun et al., 2009; Hooper et al., 2016; Almagro Armenteros et al., 2019). Dicotyledonous RFS proteins tended to hold predicted localizations in the cytosol, whereas prediction tools for the monocotyledonous RFSs gave conflicting results (Supplemental Table S1). Proteomics datasets provided little insight because only a single proteomics study identifying an RFS protein was found in the literature, a study of isolated plasma membrane from Arabidopsis cell suspension culture which identified low levels of AtRFS2 (Mitra et al., 2009). Since public databases and prediction tools provided limited and conflicting information on possible subcellular localization, we experimentally tested localization with AtRFS1-tagged N- or C-terminally with GFP (GFP-AtRFS1 and AtRFS1-GFP, respectively), introduced transiently into *Nicotiana benthamiana* leaves. Both fusion orientations demonstrated patterns consistent with localization in the ER network and, to a lesser extent, cytosol (Figure 2; Supplemental Figure S6). Notably, BdRFS protein was localized in ER and cytosol, consistent with AtRFS1 (Figure 2; Supplemental Figure S6).

Overexpression of the *BdRFS* gene delays flowering and enhances drought tolerance

To elucidate the function of *BdRFS* in *B. distachyon*, we generated constitutive overexpressor lines. RT–qPCR analysis revealed that *BdRFS* transcript was significantly (approximately four-fold) elevated in four independent transgenic lines (Figure 3B). Flowering time and senescence were greatly delayed in the *BdRFS* overexpressor lines (Figure 3, A and C; Supplemental Figure S7). For example, panicles of wild-type control were visible by ∼66 days after sowing (DAS), while those of OX2 appeared after only ∼107 DAS. Plants with delayed flowering time produce greater biomass, a desired trait for grazing operations and biofuel feedstocks (Hilbert et al., 1981; Schwartz et al., 2010). The shoot dry weight of overexpressors was significantly increased compared to wild-type (Figure 3D). Photosynthetic pigment levels of overexpressors were unchanged, except for a slight but significant increase of plastoquinone-9, which could be in favor of preventing photooxidative damage to thylakoid membranes (Supplemental Figure S8A; Supplemental Table S2). Because *BdRFS* was strongly suppressed by dehydration (Figure 1I), we next examined the drought stress response of *BdRFS* overexpressing lines. Five-week-old *B. distachyon* plants in the vegetative growth phase were deprived of water for 2 weeks and then re-watered for 3 days. Wild-type plants exhibited an extremely dehydrated phenotype, marked by dry, necrotic leaf tissue, whereas the leaves of overexpressors remained vigorous throughout the treatment interval

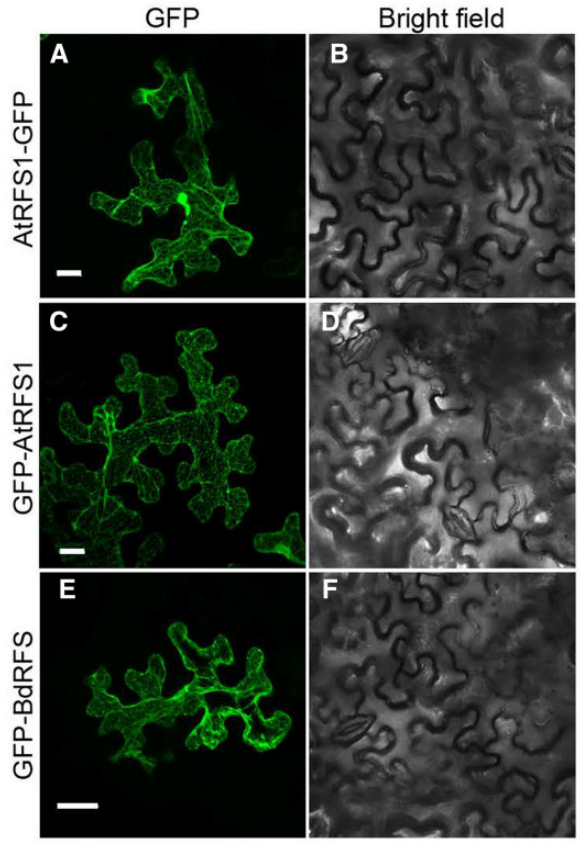

Figure 2 Subcellular localization of GFP-tagged RFS proteins in *N. benthamiana* leaf epidermal cells. GFP-fused constructs of AtRFS1 (At3g43110) (A–D) or BdRFS (Bd4g31140) (E and F) are transiently expressed in *N. benthamiana* leaves. After 48-h postinfiltration, green fluorescence was imaged. Scale bar, 20 μm.

(Figure 3E). After recovery, overexpressors restored growth, but wild-type died (Figure 3F). Notably, the leaves of overexpressors were significantly thicker than those of wild-type and had a higher leaf relative water content (RWC) during drought stress (Figure 3, G and H). Overall, the results suggest that *BdRFS* not only affects plant flowering time and vegetative biomass production but also promotes robust tolerance to drought stress.

Knockout mutants of *RFS* exhibit earlier flowering and hypersensitivity to water stress

To further investigate its biological functions, we generated *BdRFS* knockout mutants in *B. distachyon* using CRISPR/Cas9. Two single guide RNAs (sgRNA) sequences targeting the second and third conserved domains of *BdRFS* were designed by CRISPR-P (Supplemental Figure S9A). Both sgRNAs were simultaneously constructed into the pRGEB32 vector and introduced into wild-type *B. distachyon* BD21-3 calli via *Agrobacterium*-mediated transformation. Hygromycin-resistant transformants were selected for further propagation. The effects of *BdRFS* gene editing were determined by PCR analysis and confirmed by sequencing. Two independent *BdRFS* CRISPR-edited knockout mutant lines (CRISPR-ko) were selected for downstream characterization (Supplemental Figure S9B). The first line, *crispr*#3, was the result of a 1-nucleotide (nt) insertion (Adenine, A) at position 366 bp of the coding region, causing an early stop codon at amino acid position 130. The other mutant, *crispr*#9, contained a 180-nt deletion between the two sgRNAs, resulting in partial deletion of conserved domains 2 and 3.

Brachypodium distachyon CRISPR-ko mutants displayed a semi-dwarfed phenotype, earlier flowering, and reduced biomass accumulation (Figure 4, A–D; Supplemental Figures S7 and S10). The accelerated flowering phenotype of CRISPR-ko mutants was also observed when grown under an extra-long day (20-h light and 4-h dark) photoperiod (Supplemental Figure S11), indicating that the *BdRFS* gene prolongs flowering time without disturbing photoperiodism. RT–qPCR analysis showed that expression of the *FT* homologs, *BdFT1* (Bd1g48830) and *BdFT2* (Bd2g07070), were slightly increased in *crispr*#9, but not significantly (Supplemental Figure S12). Photosynthetic pigments were reduced in mature leaves of CRISPR-ko mutants (Supplemental Figure S8B; Supplemental Table S2). However, photosynthetic parameters such as Phi2 (Quantum yield of Photosystem II) and Fv/Fm (the maximum potential quantum efficiency of Photosystem II) were unaffected (Supplemental Figure S13).

Drought stress experiments revealed that the CRISPR-ko mutants were hypersensitive to water stress (Figure 4E). After withholding water for 7 days, the leaves of knockout mutants already exhibited severe wilting and dehydration symptoms in sharp contrast to wild-type plants. The leaves of *crispr*#3 were slightly thinner than those of wild-type, but the leaf RWC of the two CRISPR-ko mutants were unchanged (Figure 4, F and G). We also examined the levels of hydrogen peroxide (H_2O_2) and malondialdehyde (MDA) in leaves of wild-type and CRISPR-ko mutants. Leaves were sampled at the same developmental stage (i.e. bolting day), to exclude developmental effects. 3,3′-diaminobenzidine (DAB) staining indicated that H_2O_2 levels were increased in CRISPR-ko mutants under standard growth conditions (Figure 4H). MDA is one of the end products of PUFA peroxidation, and its level reflects oxidative stress status (Draper and Hadley, 1990). The CRISPR-ko mutants accumulated more MDA (Figure 4I), indicating that either the antioxidant systems were impaired, or reactive oxygen species generation was elevated in knockout mutants (Figure 4I). Thylakoid-associated plastoglobules (PGs) are monolayer lipid droplet particles of chloroplasts. The size and density of PGs can vary substantially under adverse conditions (van Wijk and Kessler, 2017). Transmission electron microscopy (TEM) revealed that the density, but not the size, of PGs was significantly increased in CRISPR-ko mutants (Figure 4, J and K). Together, the results suggest that *BdRFS* is a stress-inducible regulator of plant flowering time and drought tolerance.

To investigate the conservation of function among the *RFS* family, we isolated T-DNA single mutants of the two Arabidopsis homologs, At3g43110 (*atrfs1*) and At5g20790

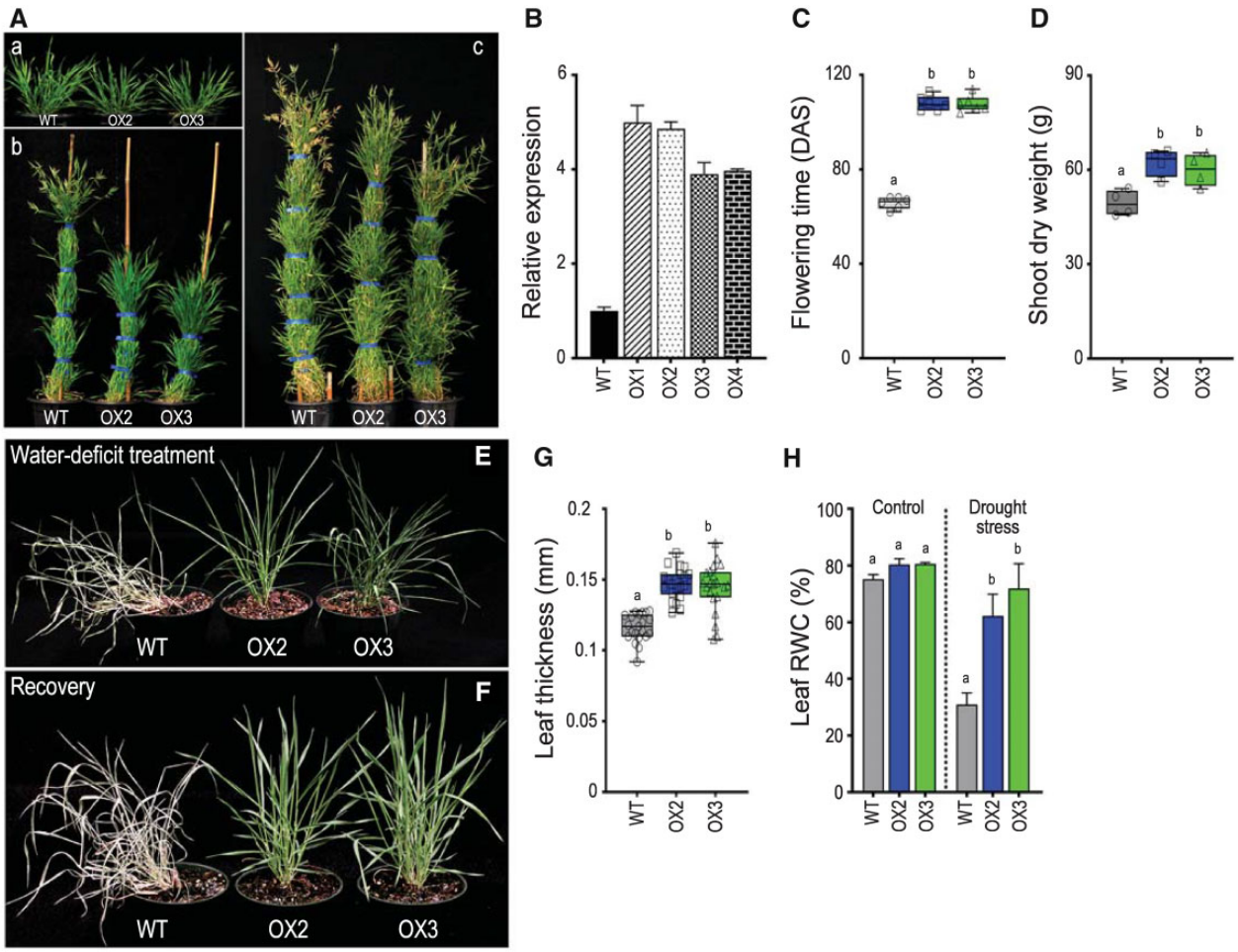

Figure 3 Phenotypes of *BdRFS* overexpression lines. A, Representative phenotypes of BD21-3 (WT) and two *BdRFS* overexpressors (OX) under long-day growth conditions. Plants are ~35 (a), 100 (b), and 135 (c) days old, respectively. B, RT–qPCR analysis of *BdRFS* (Bd4g31140) transcript levels in WT and OX lines. The *BdUBC18* gene was used as reference housekeeping gene for normalization of RT–qPCR values. The data represent the mean values of three replicates ±1 SD. C, Flowering time of WT and OX lines ($n = 6$). D, Shoot dry weight of matured WT and *BdRFS* overexpressors ($n = 4$). E and F, Representative phenotypes of WT and overexpressor lines under drought stress for 2 weeks (E), and after re-watering for 3 days (F). G, Leaf thickness of WT and overexpressor lines ($n = 21$). H, Leaf RWC% of WT and overexpressors under control (well-watered) or drought stress. The data represent the mean values of three replicates ±1 SD. For (C), (D), and (G), box limits indicate 25th and 75th percentiles, horizontal line is the median, and whiskers display minimum and maximum values. Statistical significance of differences is tested by one-way ANOVA analysis ($P < 0.001$) and is indicated by lower-case letters.

(*atrfs2*), and generated a corresponding double homozygous mutant (*dmu*) by crossing (Supplemental Figure S14A). No obvious morphological differences were observed from seedlings of single and double mutants under P-replete or -deficient conditions (Supplemental Figure S14B). However, we noticed that *dmu* bolted earlier than wild type or single mutants (Figure 5, A and B). The number of rosette leaves at bolting, and mature plant height, did not show any significant differences (Figure 5C; Supplemental Figure S14C). Notably, *dmu* exhibited water deficit sensitivity (Supplemental Figure S14D), which is consistent with the observation in the *B. distachyon* CRISPR-ko lines. Thus, the Arabidopsis *RFS* genes synergistically affect the transition to reproductive growth and drought tolerance, comparable to the role of the *B. distachyon* homolog.

Alterations to *RFS* gene expression affect lipid composition and lipid acyl-group composition

Previous studies have shown that changes in PC content in total lipids affect plant flowering/heading time (Nakamura et al., 2014; Qu et al., 2021). Furthermore, the accumulation of MDA in CRISPR-ko mutants suggested that unsaturated membrane lipids might be subjected to peroxidation and destabilization. To investigate if changes to lipid composition may underlie the developmental phenotype, we investigated the lipid profiles of the *BdRFS* CRISPR-ko mutant lines and overexpressors. Although the total free FA content of CRISPR-ko mutants did not change compared to wild type (Figure 6A), in *crispr#9*, the DGDG content was significantly reduced, while the PC content was increased (Figure 6B). The distribution of acyl groups of free FAs was altered in

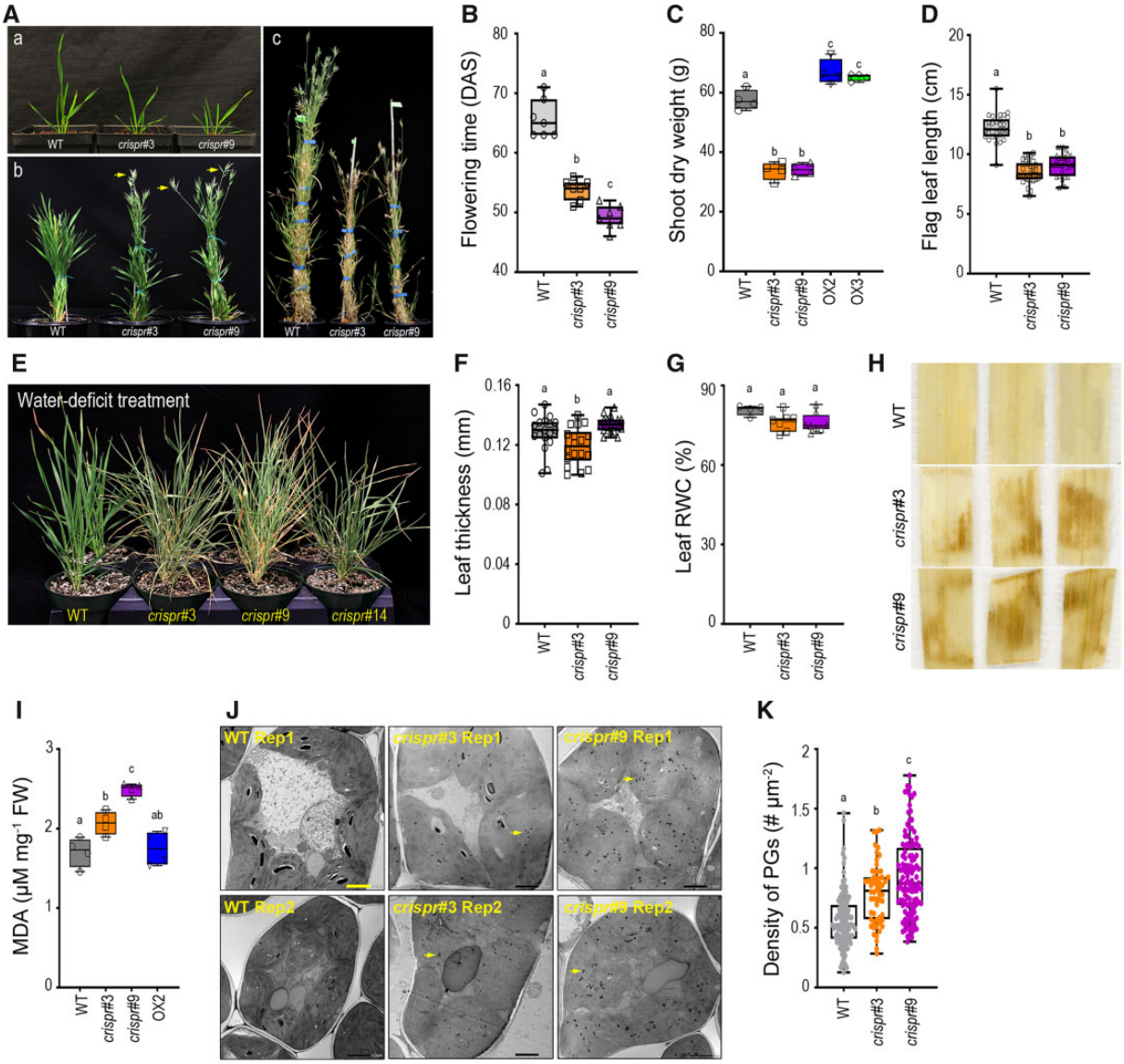

Figure 4 Phenotypes of *BdRFS* CRISPR-ko mutants. A, Representative phenotypes of WT (BD21-3; WT) and two *BdRFS* CRISPR-ko mutants under long-day growth conditions. Plants are ∼20 (a), 50 (b), and 110 (c) days old, respectively. Arrows point to spikes. B, Flowering time of WT and CRISPR mutants (n = 7). C, Shoot dry weight of matured WT and CRISPR-ko mutants (n = 4). D, Flag leaf length (n = 30), (F) leaf thickness (n = 21), and (G) leaf RWC (n = 4–7) of matured WT and CRISPR-ko mutants. E, Representative phenotype of WT and CRISPR-ko mutants after water deprivation for 7 days. H, DAB staining of leaves of WT and CRISPR-ko mutants. Scale bar, 5 mm. I, Quantification of MDA contents in wild-type, CRISPR-ko mutants, and OX2 (n = 4). J, Representative TEM micrographs illustrating chloroplast ultrastructure of wild-type and CRISPR-ko leaves. Arrows point to plastoglobules (PGs). Scale bar, 2 μm. K, Numbers of PGs per chloroplast area in WT and CRISPR-ko mutants. Measurements are collected from 10 micrographs of four different plants each, per genotype. All experiments are repeated 3 times and representative results are presented in the figure. For (B), (C), (D), (F), (G), (I), and (K), box limits indicate 25th and 75th percentiles, horizontal line is the median, and whiskers display minimum and maximum values. Statistical significance of differences is tested by one-way ANOVA analysis ($P < 0.001$) and is indicated by lower-case letters.

each lipid class, with a slight but significant decrease in C18:3 and an increase in C16:0 (Supplemental Figure S15A; Supplemental Table S3). For instance, the C16:0 level in PC of *crispr*#9 was ∼10% more than that of the wild-type (Figure 6D). Moreover, C18:0 level in DGDG was also increased in *crispr*#9 (Figure 6C). The double bond index (DBI) reflects the degree of unsaturation of membrane lipids. The DBI levels of CRISPR-ko mutants were significantly lower than wild type (Supplemental Figure S15B).

In contrast, OX3 had significantly lower total FA content than the wild type (Figure 6F). The DGDG content of OX3 was increased, while its PC content was decreased, the reverse of the pattern observed in the CRISPR-ko mutants (Figure 6G). Reciprocal alteration of PC and DGDG levels is repeatedly observed in P-starved plants (Pfaff et al., 2020; Sun et al., 2020). Alterations to DGDG content consequently affected the MGDG/DGDG ratio (Figure 6, E and J). Levels of C18:2 in total FAs were significantly increased in

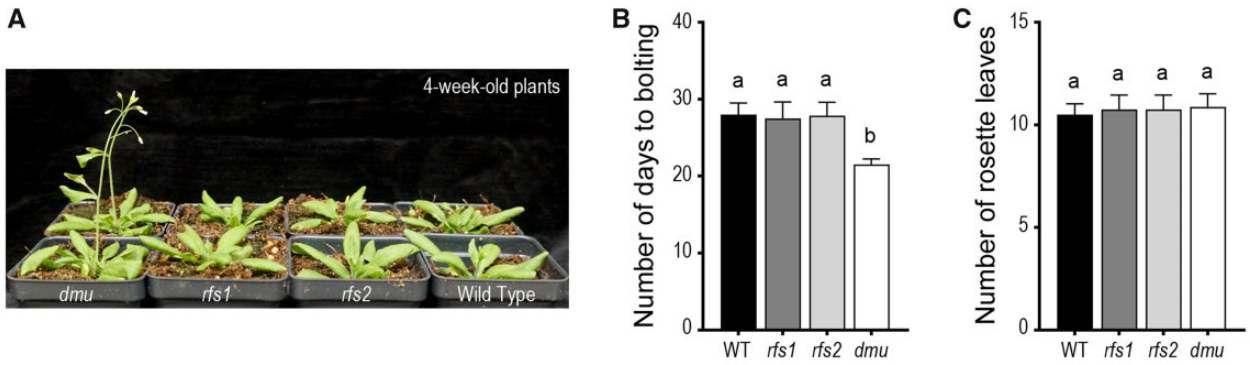

Figure 5 Effects of loss of *AtRFS1* and *AtRFS2* on bolting time in Arabidopsis. A, Representative image showing the bolting phenotype of *Atrfs1*, *Atrfs2*, and the corresponding double mutant (*dmu*) in Arabidopsis. Seedlings were germinated on 1/2 MS solid medium for 7 days, then transferred to soil to grow until senescence. B, Bolting time of various genotypes. C, Total rosette leaves numbers of various genotypes at bolting. The data represent the mean values of ten replicates ±1 SD. Statistical significance of differences is tested by one-way ANOVA analysis ($P < 0.001$) and is indicated by lower-case letters.

overexpressor lines (Supplemental Figure S15C; Supplemental Table S4). Additionally, in OX3, the level of C16:0 in DGDG was substantially decreased, whereas the C18:2 and C18:3 levels were significantly increased (Figure 6H). The level of C18:2 in PC was also increased, but C18:0, C18:1, and C18:3 levels were noticeably decreased (Figure 6I). Notably, the DBI levels of overexpressors were comparable to wild type (Supplemental Figure S15D).

In addition, we examined the lipid profiles of the *atrfs* double mutant (*dmu*), which exhibited the earlier bolting (transition to reproductive growth) phenotype (Figure 5A). Compared to wild-type (Col-0), *dmu* contained a higher total lipid content, but its relative proportions of lipid classes were unchanged (Figure 6, K and L). The abundance of C16:3 in DGDG was decreased in *dmu* (Figure 6M; Supplemental Table S5). Similar to *B. distachyon crispr*#9, levels of C16:0 and C18:3 in PC were, respectively, increased and decreased in *dmu* (Figure 6N). The MGDG/DGDG ratio of *dmu*, however, did not change (Figure 6O). Collectively, the results suggest that plant *RFS* genes affect polar lipids, particularly the acyl chain composition, in a specific and conserved manner.

Endogenous JA abundance is reduced in *BdRFS* CRISPR-ko mutants

The PUFA, α-linolenic acid (C18:3), is the precursor of jasmonic acid (JA) biosynthesis (Wasternack and Song, 2016). Because the level of C18:3 FA was decreased in CRISPR-ko mutants, we hypothesized that the JA and related metabolites might be reduced as well. To test this hypothesis, we examined endogenous phytohormones from different genotypes. Despite no change in the 12-oxophytodienoic acid (OPDA, intermediate of JA biosynthesis) level (Figure 7A), levels of JA, MeJA, and JA-Isoleucine (JA-Ile) were reduced in *crispr*#9 compared with that in the wild type (Figure 7, B–D). However, the JA and JA-Ile levels were not altered in overexpressors (Figure 7, E and F). Next, we selected four *B. distachyon* JA-inducible genes, *BdJAZ* (Bd3g23190), *BdLOX* (Bd1g11670), *BdMYC2* (Bd3g34200), and *BdOPR3* (Bd3g37650) based on previous studies (Kakei et al., 2015; Kouzai et al., 2016) and examined their transcriptional changes after a MeJA treatment, to determine whether JA signaling in *crispr*#9 was altered. Similar to the responses in wild-type, all tested genes were upregulated after MeJA treatment (Figure 7, G–J), indicating that JA signaling was unaffected in *crispr*#9. The results suggest that *BdRFS* affects JA biosynthesis but not signal transduction.

Identification of candidate interacting proteins of BdRFS

To reveal the molecular mechanisms underlying the role of BdRFS, we performed co-immunoprecipitation (Co-IP) to identify putative protein interactors. Due to high insolubility of the full-length heterogeneously expressed BdRFS protein, even with an N-terminal SUMO tag, we deleted the first 45 amino acids of BdRFS encompassing its predicted transmembrane domain (Supplemental Figure S3B). Solubility was greatly improved in this truncated form (His-SUMO-BdRFS$^{\Delta 1\text{-}45}$) and hence was used for the subsequent Co-IP assay alongside an empty His-SUMO tag as negative control. Proteins were incubated with crude protein extracts from mature wild-type leaf tissue and eluates were analyzed by LC–MS/MS (tandem mass spectrometry). A total of 46 potential interactors were identified specifically in the presence of BdRFS$^{\Delta 1\text{-}45}$ (Table 1; Supplemental Table S6). Remarkably, the highest abundant candidate interactor was ABA-, Stress-, and Ripening-induced 2 (BdASR2, Bd4g24650), homologs of which are positive regulators of drought stress tolerance with very similar overexpression phenotypes to the BdRFS overexpressor lines (Wang et al., 2016; Yoon et al., 2019, 2021; Qiu et al., 2021). Also of particular interest, PLD α1 (BdPLD α1, Bd2g04480) was identified as a putative BdRFS-interacting protein. The Arabidopsis PLD α1 preferentially hydrolyzes PC to phosphatidic acid (PA), and the latter acts as an essential lipid signaling molecule in regulation of freezing or drought stress and ABA responses (Wang, 2005; Wang et al., 2014; Hong et al., 2016; Takáč et al., 2019). Furthermore, overexpression of AtPLD α1 substantially

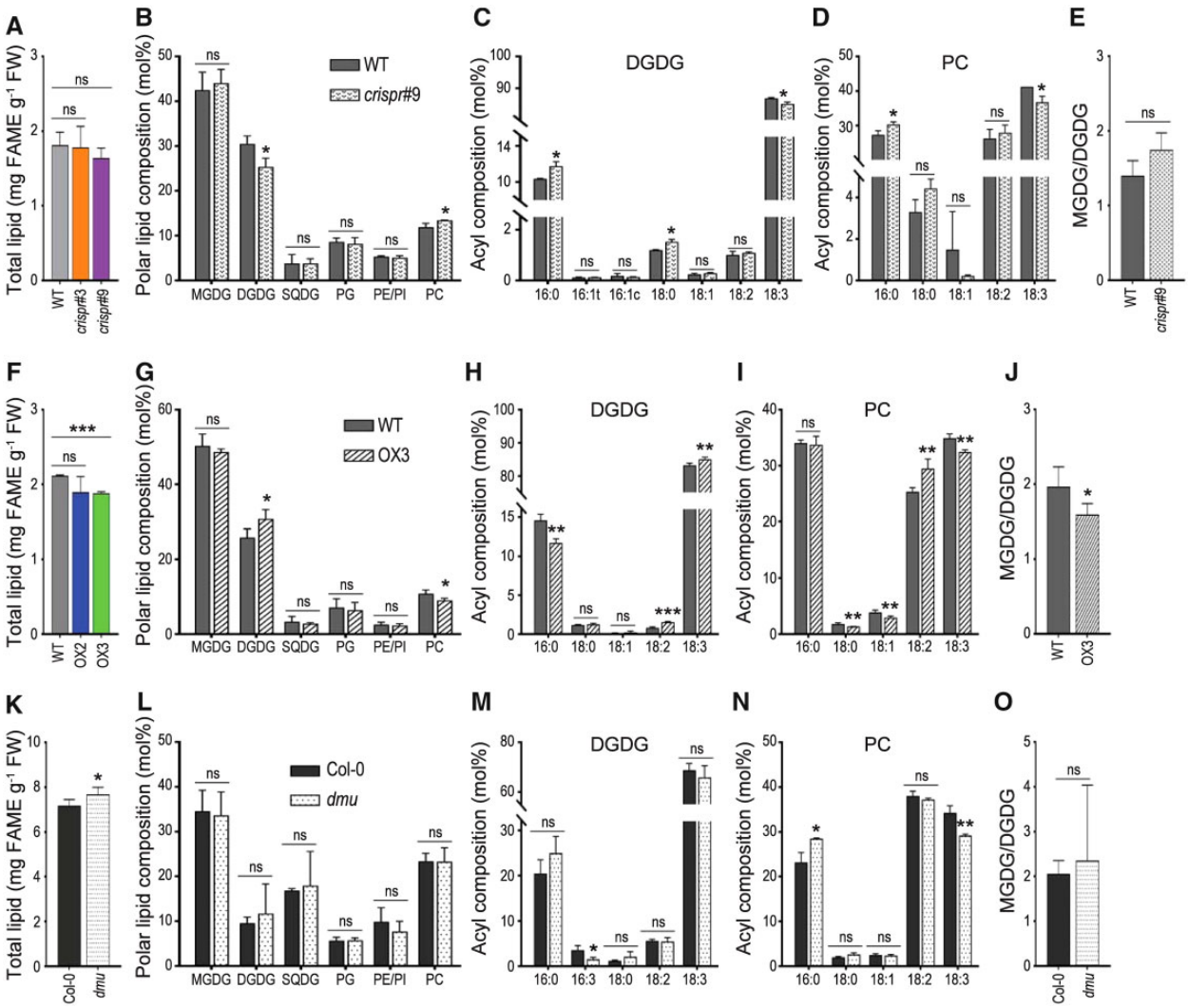

Figure 6 Lipid analysis of *BdRFS* CRISPR-ko mutants and overexpression lines, and the Arabidopsis *RFS* double mutant (*dmu*). A–E, total lipids content (A), lipid composition (B), acyl group distributions of DGDG (C) and PC (D), and ratio of MGDG to DGDG (E), in leaves of WT (BD21-3) and CRISPR-ko mutants grown under long-day conditions. F–J, total lipid content (F), lipid composition (G), acyl group distributions of DGDG (H) and PC (I), and ratio of MGDG to DGDG (J), in leaves of WT (BD21-3) and overexpressor lines grown under long-day conditions. K–O, total lipid content (K), lipid composition (L), acyl group distributions of DGDG (M) and PC (N), and ratio of MGDG to DGDG (O), in shoots of Arabidopsis WT (Col-0) and the *AtRFS* double mutant (*dmu*) grown in growth chamber. A, F, and K, the data represent the mean values of three replicates ±1 SD, statistical significance of differences is tested by one-way ANOVA analysis ($P < 0.05$) and is indicated by lower-case letters. B–D, G–I, and K–O, the data represent the molar ratio of total lipids and represent the mean values of three replicates ±1 SD. Acyl groups are designated with numbers of carbons:number of double bonds. *$P < 0.05$, **$P < 0.01$, and ***$P < 0.001$ indicate statistical significance as determined by Student's *t* test. NS, no significance.

enhances drought tolerance by regulating ABA-dependent stomatal movements and transpirational water loss (Sang et al., 2001; Hong et al., 2008a, 2008b, 2008c). Notably, six different putative interacting proteins are associated with ABA signaling or biosynthesis, including the two aforementioned proteins, BdASR2, and BdPLD α1 (Table 1).

Discussion

Here, we report a widely conserved and stress-inducible single pass transmembrane gene family in plants, which we name the *RFS* family. Knockout of the *RFS* homologs in Arabidopsis and *B. distachyon* result in an earlier transition to reproductive growth, a reduced growth rate, and hypersensitivity to water stress, while *BdRFS* overexpressor lines exhibit delayed transition to reproductive growth, increased biomass accumulation, and enhanced drought tolerance. The reciprocity of phenotypes seen between overexpressor and CRISPR-ko lines in *B. distachyon*, as well as the complementarity between Arabidopsis and *B. distachyon* T-DNA/CRISPR-ko lines, indicate a conserved role for this gene family in growth, development, and stress tolerance. Furthermore, specific and reproducible effects on the abundance and acyl chain composition of PC and DGDG indicate

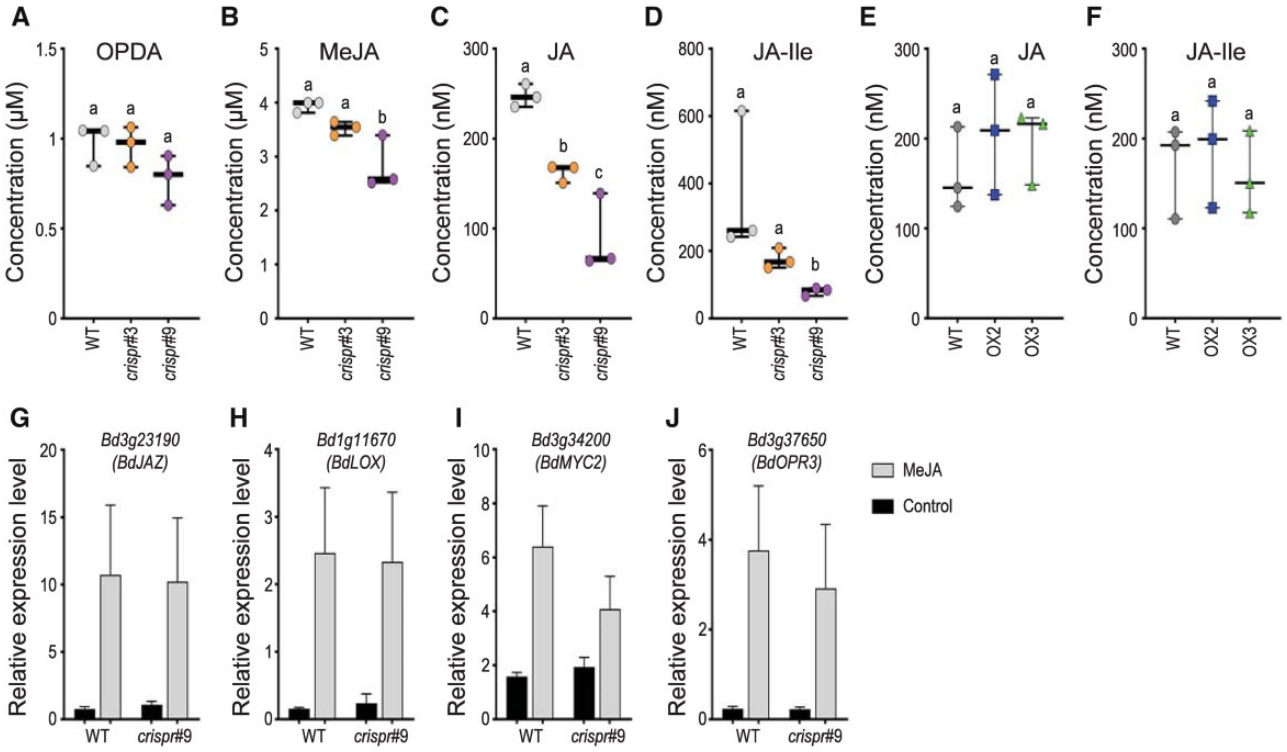

Figure 7 Reduction of endogenous JA and related metabolites in *BdRFS* CRISPR-ko mutants. A–D, quantification of OPDA (A), MeJA (B), jasmonate (JA) (C), and JA-Ile (D) in mature leaves of WT (BD21-3) and CRISPR-ko lines grown under long-day conditions. E and F, quantification of JA (E) and JA-Ile (F) in mature leaves of WT (BD21-3) and overexpressor lines grown under long-day conditions. G–J, expression analysis of JA-inducible genes, *BdJAZ* (Bd3g23190) (G), *BdLOX* (Bd1g11670) (H), *BdMYC2* (Bd3g34200) (I), and *BdOPR3* (Bd3g37650) (J), in WT (BD21-3), and *crispr*#9, under MeJA treatment. The data represent the mean values of three replicates ±1 SD. All experiments were repeated 3 times and representative results are presented in figures. For (A)–(F), box limits indicate 25th and 75th percentiles, horizontal line is the median, and whiskers display minimum and maximum values. Statistical significance of differences is tested by one-way ANOVA analysis ($P < 0.05$) and is indicated by lower-case letters.

that a role of *RFS* homologs in lipid metabolism may underlie the phenotypic patterns seen at the whole plant level.

Our analysis of gene expression patterns among *RFS* members of diverse species suggests that they are coordinated with the dynamic changes in phospholipid abundance, consistent with their impact on phospholipids in the CRISPR-ko and overexpressor mutant lines (Figures 6 and 8; Supplemental Figure S15; Supplemental Table S3). Phospholipids are indispensable components of biological membranes, and their prevalence and chemical composition change when plants adapt to adverse conditions. Indeed, during P-stress, the Arabidopsis PHR1 TF activates the expression of lipid remodeling genes to regulate phospholipid degradation (Rubio et al., 2001; Pant et al., 2015). Expression analysis confirmed that plant *RFS* gene expression was dependent on PHRs and that they show conservation of abiotic stress responses across multiple monocot and dicot species as well (Figure 1F; Supplemental Figures S4, C, F–H). Similar effects on phospholipid metabolic genes and bulk membrane lipid composition are seen in response to drought or freezing stresses when adjustments to membrane lipid composition are critical to protect cellular membrane stability (Vigh et al., 1986; Welti et al., 2002; Kong et al., 2019). Moreover, phospholipid composition fluctuates diurnally (Browse et al., 1981; Nakamura et al., 2014; Nakamura, 2018). Notably, we found that the *OsRFS* transcript also cycled diurnally (Supplemental Figure S4D), comparable to findings for the *BdRFS* transcript (Koda et al., 2017). Furthermore, it is of interest that young and expanding leaves have higher phospholipid content than mature leaves in *Banksia* and *Hakea* species (Lambers et al., 2012). This is the opposite trend as the expression pattern of the *OsRFS* and *ZmRFS* genes along the leaf developmental gradient (Supplemental Figure S5), suggesting a negative effect of *RFS* homologs on phospholipid accumulation.

In addition to the relevance of PC to membrane properties and stress tolerance, PC levels in Arabidopsis and *O. sativa* can substantially affect flowering time; in fact, FT protein homologs exhibit high affinity for C16:0-containing PC (Nakamura et al., 2014; Qu et al., 2021). Because expression of *BdFT1* and *BdFT2* were unchanged in *crispr*#9 (Supplemental Figure S12), we conclude that the altered flowering time in *BdRFS* transgenic lines was not due to altered FT levels *per se*. Instead, the elevated levels of PC, especially PC C16:0-containing species, in *crispr*#9 might promote FT–PC interactions and lead to stronger activation of FT signaling and the precocious flowering phenotype. In contrast to the CRISPR-ko mutant, PC level was significantly

Table 1 Selected candidate interacting proteins of BdRFS determined by Co-IP

Protein ID	Annotation	Eluate (BdRFS)[a]	Eluate (Neg Ctrl)[a]	Input[a]	Notes
Bradi4g24650	ASR2 (Abscisic acid-, stress-, and ripening-induced 2)	51,856,000	–[b]	–[b]	Responsive to ABA and various abiotic stresses; overexpression of a wheat homolog in *B. distachyon* strongly promotes drought stress tolerance and ABA accumulation
Bradi2g01850	LPR2 (Low Phosphate Root 2; cupredoxin family)	25,251,000	–[b]	–[b]	Responsive to P-starvation; adjusts root meristem activity; copper oxidase domain
Bradi5g12120	PLAT1 (Polycystin, Lipoxygenase, Alpha-toxin, and Triacylglycerol lipase 1)	22,478,000	–[b]	–[b]	Lipase/lipoxygenase-like protein; responsive to various (a)biotic stresses
Bradi4g00330	NCED1 (Nine-cis Epoxycarotenoid Cleavage Dioxygenase 1)	14,836,200	–[b]	–[b]	Committed enzymatic step of ABA biosynthesis
Bradi2g04480	PLD-α1	9,165,100	–[b]	6,092,600	Responsive to ABA signaling, and positive regulator of ABA signaling; cleaves terminal phosphodiester bond of phospholipids to generate PA

[a]Average LFQ intensity from two bioreplicates.
[b]Not detected.

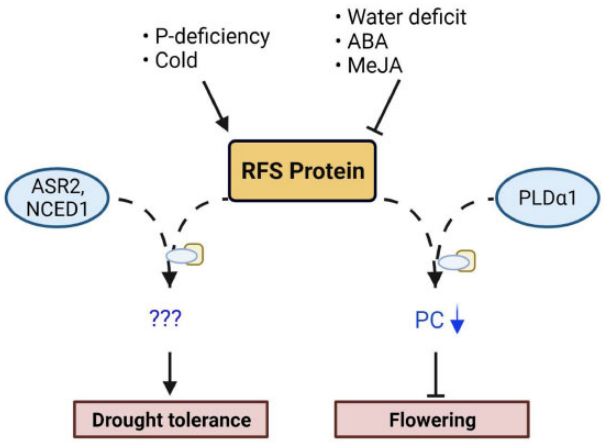

Figure 8 A working model of the role of RFS in drought tolerance and flowering time that summarizes reported results. The RFS genes are induced by P-deficiency and cold stress and conversely are suppressed by water deficit, ABA treatment, and MeJA treatment. RFS induces polar lipid remodeling, including suppressed levels of PC containing C16:0 which, in turn, inhibits flowering. We propose that this effect on the lipid composition is achieved through a direct interaction with PLDα1. Furthermore, we suggest that direct interactions of RFS with other abiotic stress-related proteins such as ABA-, stress-, and ripening-related 2 (ASR2), or Nine-cis Epoxycarotenoid Cleavage Dioxygenase 1 (NCED1) works to promote drought tolerance through as yet unknown mechanisms. If such an effect operates through promotion of ABA biosynthesis/accumulation, then this could represent a feedback inhibition loop through the demonstrated downregulation of *RFS* transcript.

decreased in *BdRFS* OX lines, in which flowering time was delayed (Figure 6, D and I). During many stresses, plants accelerate flowering to conclude the life cycle and complete seed production before damage can prevent effective seed set (Riboni et al., 2013; Chong et al., 2022). Given that *BdRFS* is strongly suppressed by drought stress, and the CRISPR-ko mutants exhibit an early flowering phenotype, we suggest that *BdRFS* may function by accelerating flowering time through upregulation of PC levels (particularly those containing C16:0 acyl chains) in response to water deficit. In addition, long-day plants such as *B. distachyon* have evolved mechanisms to prevent flowering under low temperature, thereby protecting floral meristems from cold damage. Thus, the freezing stress-inducible characteristic of *BdRFS* might contribute to the suppression of winter flowering through the downregulation of PC, as seen in the overexpressor lines. In this regard, it is notable that BdPLD α1 was identified as a potential interactor of BdRFS because the AtPLD α1 homolog prefers PC as a substrate (Wang et al., 2014). In light of this finding, coupled with the lipid remodeling effects reported above, it is plausible that BdRFS may enhance the activity of BdPLD α1 through direct interaction, providing a mechanism by which PC content is modified by RFS levels. We could not find reports of flowering-time phenotypes among PLD α1 knockout or overexpression lines. However, AtPLD α3 accelerated flowering time specifically under water-deficit conditions (Hong et al., 2008a, 2008b, 2008c) while a secreted PLD in rice was found to delay flowering by acting on PC (Qu et al., 2021). A proposed model of RFS effects on drought tolerance and flowering, summarizing the findings reported in this work, is presented in Figure 8.

JA is involved in many aspects of plant development and stress responses, through the SCF^{COI}-JAZ-MYC signaling cascade (Wasternack and Song, 2016). JA content is positively associated with drought tolerance, biomass yield, and entry into senescence (Fisher et al., 2016; Raza et al., 2021). C18:3 of chloroplast galactolipids is the substrate for JA biosynthesis (Li and Yu, 2018; Cook et al., 2021). Thus, it is notable that the reduction of C18:3 in *crispr*#9 corresponded with reductions in JA content and biomass accumulation (Figures 4, C and 7, B–D; Supplemental Figure S7).

Endogenous levels of JA (and related metabolites) are rhythmic and peak during the day, which correspond with changes in *RFS* gene expression (Figure 1H; Supplemental Figure S4D).

Although further biochemical study is required to delineate the underlying molecular function and regulation of the RFS proteins, our results demonstrate that this family represents a stress-inducible orchestrator of flowering/heading time, growth rate, and stress tolerance, likely through their effect on polar lipid content and acyl composition. The potential to deploy RFS in crop improvement is readily apparent, as indicated by the overexpression of *BdRFS* in *B. distachyon*, which substantially enhances water-deficit stress tolerance with simultaneous promotion of biomass accumulation. Hence, our results reveal a potentially valuable tool for biotechnological improvement of drought resilience in agricultural crops, as well as improved biomass accumulation of forage grasses and biofuel feedstocks.

Materials and methods

Plant material, growth, and treatment

Arabidopsis (*A. thaliana*) ecotype Col-0 seeds were sterilized and planted as described by Ying et al. (2022). Arabidopsis bolting time was monitored daily and determined as the number of days from sowing to the first elongation of the floral stem at 1-mm height. The T-DNA insertion mutant line of At3g43110 (*atrfs1*, GK-422C11) and At5g20790 (*atrfs2*, SALK_030486) were obtained from GABI-Kat (Kleinboelting et al., 2012) or Arabidopsis Biological Resource Center, respectively. Homozygous mutant plants were identified or validated according to the SiGnAL database PCR-based protocol (http://signal.salk.edu/).

Brachypodium distachyon ecotype BD21-3 seeds were surface sterilized by solution containing 30% (v/v) bleach and 0.05% (v/v) Tween-20, then stratified for 3 days in the dark at 4°C, and germinated on 1/2 murashige and skoog agar (1% w/v) plates. Plants were cultured vertically in growth chamber (175-μmol^{-2} s^{-1} light intensity, 22°C/18°C, 16-h light and 8-h dark cycle) for 7 days, then transplanted into the soil (SureMix) and grown in greenhouse (24°C, 16-h light and 8-h dark cycle) until plants were matured. Leaf samples of mature plants were harvested for phenotypic, biochemical, or molecular examination. Leaf thickness was measured by using a digital micrometer. For P-limitation treatment, sterilized seeds were directly placed on 1/2 MS agar containing 675 or 0-μM phosphate and grown vertically in the growth chamber for 10 days. For dehydration treatment, 3-week-old seedlings were taken immediately out from pots and placed on the Whatman 3MM paper to dry at ambient temperature for 6 h. For freezing treatment, the seedlings at the same development stage were transferred to a growth chamber at −4°C for 6 h. For phytohormone treatments, 100 μM of ABA or MeJA was sprayed on the leaves of 3-week-old BD21-3 seedlings and covered with plastic wrap for 30 min. For tunicamycin (Tm) treatment, 7-day-old BD21-3 seedlings were transferred to 1/2 MS agar supplemented with 50-ng mL^{-1} Tm and grown vertically in the growth chamber for 3 h. Target tissues were sampled at an indicated time point, quickly frozen in liquid N_2, and stored at −80°C for further studies.

RT–qPCR

Total RNA was extracted and RT–qPCR was conducted as described by Ying et al. (2022). The Arabidopsis *GAPDH* (At1g13440) or *B. distachyon UBC18* (Bd4g00660) gene was used as an internal control (Czechowski et al., 2005; Hong et al., 2008a, 2008b, 2008c). All the experiments were repeated at least 3 times using cDNAs prepared from two different biological replicates with representative results shown in the figures. Sequences of primers used in the study are listed in Supplemental Table S7.

Identification and phylogenetic analysis of RFS proteins

To search RFS proteins from different plant species, a BLASTP search was conducted on the Phytozome version 13 (Goodstein et al., 2011) website using the C-terminal conserved domain of At3g43110 protein as query sequence. Identified protein sequences with low E-value (<0.001) were downloaded and aligned using the MUSCLE algorithm with the MEGA X software (Kumar et al., 2018). A phylogenetic rooted tree was constructed with MEGA X software by using the UPGMA algorithm with the default settings. Bootstrapping was performed 1,000 times. The inferred trees were visualized using iTOL (Letunic and Bork, 2021).

Generation of transformants

For histochemical GUS analysis of Arabidopsis *RFS* genes, 1,561-bp or 486-bp upstream (from start codon) fragment of At3g43110 or At5g20790 gene was amplified from genomic DNA, subcloned into pENTR/D-TOPO Gateway entry vector (Invitrogen, Waltham, MA, USA), and finally introduced into the vector pBGWFS7 (Karimi et al., 2002). For generation of CRISPR knockout (CRISPR-ko) mutants, two target sgRNA sequences of Bd4g31140 gene were designed by CRISPR-P version 2.0 online program (Liu et al., 2017) and constructed into pRGEB32 vector as described previously (Xie et al., 2015). For generation of overexpressor lines, the full-length coding region of Bd4g31140 gene was amplified from *B. distachyon* BD21-3 seedling cDNA, subcloned into pENTR/D-TOPO Gateway entry vector, and finally constructed into pANIC6B vector (Mann et al., 2012). Transformation procedures for Arabidopsis or *B. distachyon* were described by Ying et al. (2022).

Histochemical GUS staining

The histochemical GUS staining was performed as previously described (Ying et al., 2022). Briefly, seedlings were incubated in a GUS staining solution containing 100 mM sodium phosphate (pH 7.0), 1 mM EDTA, 0.05% (v/v) Triton X-100, 1 mM potassium ferricyanide/ferrocyanide, and 0.5 mg mL^{-1}

X-glucuronide (Goldbio) at 37°C for 1–3 h. Then samples were progressively cleared in gradient ethanol solution for 30 min. Images were acquired using a Nikon SMZ1500 stereomicroscope.

Nicotiana benthamiana infiltration and fluorescence microscopy

The full-length coding region of At3g43110 gene was ligated into pEarlyGate103 vector (Earley et al., 2006), to generate GFP-fused protein driven by CaMV35S promoter. Constructs were transformed into *N. benthamiana* using Agro-infiltration (Li, 2011). Forty-eight hours after transformation, GFP fluorescence was monitored with a Leica TCS SP8 confocal laser-scanning microscope (White Light Laser; 20% intensity; Gains, 1.0; Ex: 488 nm; Em 507 nm). All experiments have been repeated at least 3 times and representative images are displayed in figures.

TEM

The middle third of fully expanded leaves from 3-week-old *B. distachyon* plants were collected for TEM analysis. Samples (1 mm^2 size) were fixed, stained, and sectioned as described in Lundquist et al. (2013). The images were captured by a JEOL 1400 Flash TEM. Measurements of plastoglobule densities in chloroplast areas were made using ImageJ.

Extraction and quantification of JA and its derivatives

Leaf tissues were collected at the indicated developmental stages and immediately snap-frozen in liquid N_2. JAs were extracted and quantified as previously described (Havko et al., 2020). Briefly, frozen tissue was ground by TissueLyser (QIAGEN, Hilden, Germany) and extracted in cold buffer containing 80% (v/v) methanol (Millipore Sigma, Burlington, MA, USA), 0.1% (v/v) formic acid and 0.1 mg mL^{-1} butylated hydroxytoluene. (+)-ABA-d_6 (Cayman Chemical, Ann Arbor, MI, USA) was used as an internal standard. Measurements were performed by using a Xevo TQ-XS ultra-performance liquid chromatography (UPLC)/MS/MS.

Lipid analyses

Total lipid was extracted from leaf tissues of different genotypes at the same developmental stage. The procedures of extraction, thin-layer chromatography (TLC) of polar lipids, transesterification, and gas–liquid chromatography (GC) were performed as described previously (Wang and Benning, 2011; Yang et al., 2017). Briefly, lipid separation was performed by activated $(NH_4)_2SO_4$-impregnated silica gel TLC plates (TLC Silica gel 60, EMD Chemical) with a solvent consisting of acetone, toluene, and water (91:30:7.5 by volume). Lipids were visualized by brief exposure to iodine vapor on TLC plates, scraped, and converted to methyl esters, which were subsequently quantified by Agilent 7890A GC system.

For prenyl-lipid analysis, the extraction was conducted according to the previous report (Espinoza-Corral et al., 2021). Compounds were separated by using Nexera-i2040C-3D HPLC system (Shimadzu) and the concentrations were determined by using LabSolutions software (version 5.97 SP1, Shimadzu), based on calibration curves. All the experiments were repeated 3 times by using different biological replicates.

Measurement of total chlorophyll contents, MDA and RWC

For total chlorophyll measurements, 100 mg of ground leaf tissue was incubated with 10 mL of 80% acetone (v/v) at 80°C for 20 min. The absorbance of chlorophyll extraction was detected with spectrophotometer (Biotek) at 645- and 663-nm wavelength separately, and the chlorophyll content was calculated using the following formula: total chlorophyll content (mg g^{-1} fresh weight) = [20.2 × (A645) + 8.02 × (A663)] × volume/fresh weight.

The content of MDA in the leaf tissue was measured as described by Dhindsa et al. (1981). Briefly, ∼100 mg of leaf sample was homogenized in 0.8 mL 0.1% (w/v) trichloroacetic acid (TCA). The homogenate was centrifuged at 10,000*g* for 5 min. About 0.4 mL of the supernatant was mixed with 1.6 mL 20% (w/v) TCA containing 0.5% (w/v) thiobarbituric acid. The mixture was heated at 95°C for 30 min and then quickly chilled on ice. After centrifuging at 10,000*g* for 10 min, the absorbance of the supernatant was, respectively, read at 532 and 600 nm (nonspecific absorption) by using a spectrophotometer. The content of MDA (μM mg^{-1} fresh weight) was calculated as: (A532−A600) × 2/(155 × 0.1).

For leaf RWC analysis, four individual leaves from the same plant were collected together as one replicate. The RWC (%) was calculated as: 100 × (fresh weight−dry weight)/(turgid weight−dry weight). All the experiments were repeated 3 times using samples harvested from five biological replicates of each genotype.

Detection of H_2O_2

To visually detect endogenous H_2O_2, *B. distachyon* fully expanded leaves at the same developmental stage were collected and incubated in DAB (1 mg mL^{-1}, Millipore Sigma) solution for 24 h at room temperature. Leave samples were then decolorized in boiling ethanol for 30 min. Images were captured by an Epson Perfection V700 scanner. All the experiments were repeated 3 times using samples harvested from five biological replicates of each genotype.

Co-IP analysis

For heterologous expression of BdRFS, the full-length and N-terminally truncated (Δ1-45, residues 1–45, including the transmembrane domain) cDNA fragments were sub-cloned into a modified pET28b vector (New England Biolabs, Ipswich, MA, USA) carrying an N-terminal 6× His and SUMO (Small Ubiquitin-like Modifier) tag. For recombinant protein production, constructs were separately introduced into the *Escherichia coli* BL21 (DE3) pLysS competent cells (Agilent Technologies, Santa Clara, CA, USA). The

purification was performed using Ni-NTA agarose (Qiagen, Hilden, Germany) according to the manufacturer's instructions. Protein concentration was quantified using Pierce Rapid Gold BCA Protein Assay kit (Thermo Fisher Scientific), and stored in −80°C freezer for further study.

Co-IPs and crude protein extractions were carried out according to Ying et al. (2022) with minor modifications. Briefly, recombinant His-SUMO-BdRFS$^{\Delta 1\text{-}45}$ or His-SUMO protein (2 μg) were incubated with 25-μL Dynabeads His tag magnetic beads (Invitrogen) in the buffer containing 50-mM sodium phosphate (pH 8.0), 300-mM NaCl, and 0.01% (v/v) Tween-20 for 10 min at 4°C. Then, the supernatant was discarded by placing the tube on a magnet for 2 min. After 3 times washing with the same buffer, crude protein extract (10 mg) was added to the magnetic beads-recombinant protein complex and incubated on a rotator for 1 h at 4°C. The bound protein was eluted by using 100-μL elution buffer containing 50-mM sodium phosphate (pH 8.0), 300-mM NaCl, 0.01% (v/v) Tween-20, and 300-mM imidazole. Composition of the eluates and inputs were determined using LC–MS/MS as follows: proteins were loaded onto a 12.5% pre-cast BioRad Criterion 1D gel and electrophoresed at 50 V constant for ∼20 min or until the dye front migrated 2–3 mm below the well. Electrophoresis was stopped and the gel stained using Coomassie Blue. Concentrated sample bands were then excised from the gel and placed into individual microfuge tubes. Gel bands were digested in-gel according to Shevchenko et al. (1996) with modifications. Briefly, gel bands were dehydrated using 100% (v/v) acetonitrile (ACN) and incubated with 10-mM dithiothreitol in 100-mM ammonium bicarbonate, pH ∼8, at 56°C for 45 min, dehydrated again and incubated in the dark with 50-mM iodoacetamide in 100-mM ammonium bicarbonate for 20 min. Gel bands were then washed with ammonium bicarbonate and dehydrated again. Sequencing grade modified trypsin was prepared to 0.005 μg μL^{-1} in 50-mM ammonium bicarbonate and ∼100 μL of this was added to each gel band so that the gel was completely submerged. Bands were then incubated at 37°C overnight. Peptides were extracted from the gel by water bath sonication in a solution of 60% (v/v) ACN/1% (v/v) Trifluoroacetic acid (TFA) and vacuum dried to ∼2 μL. Digests were re-suspended to 20 μL in 2% (v/v) ACN/0.1% (v/v) TFA. An injection of 10 μL was automatically made using a Thermo EASYnLC 1200 onto a Thermo Acclaim PepMap RSLC 0.075 mm × 250 mm C18 column with a gradient of 5% B to 40% B in 24 min, ramping to 90% B at 25 min and held at 90% B for the duration of the run (Buffer A = 99.9% (v/v) Water/0.1% (v/v) Formic Acid, Buffer B = 80% (v/v) ACN/0.1% (v/v) Formic Acid/19.9% (v/v) Water) at a constant flow rate of 300 nL min^{-1}. Column temperature was maintained at a constant temperature of 50°C using and integrated column oven (PRSO-V2, Sonation GmbH, Biberach, Germany). Eluted peptides were sprayed into a Thermo Scientific Q-Exactive HF-X mass spectrometer using a FlexSpray spray ion source. Survey scans were taken in the Orbitrap (60,000 resolution, determined at *m*/*z* 200) and the top 15 ions in each survey scan are then subjected to automatic higher energy collision-induced dissociation with fragment spectra acquired at 15,000 resolution. The resulting MS/MS spectra are converted to peak lists using MaxQuant, version 1.6.3.4 and searched against a library containing all *B. distachyon* protein sequences available from Phytozome version 13. The MaxQuant output was then analyzed using scaffold Q + S, v5.1.2 to probabilistically validate protein identifications. Assignments validated using the Scaffold 1% false discovery rate (FDR) confidence filter are considered true. The mass spectrometry proteomics data have been deposited to the ProteomeXchange Consortium via the PRIDE partner repository (https://www.ebi.ac.uk/pride/) in MIAPE-compliant format with the dataset identifier PXD033835.

Graphs and statistical analyses

Statistical analyses and plotting were performed with GraphPad Prism version 9.3 (GraphPad Software, Inc., San Diego, CA, USA). Data on phenotypic or phytohormone measurements were subjected to statistical analysis by one-way ANOVA or Student's *t* test.

Accession numbers

Sequence data from this article can be found in the Phytozome version 13 or Ensembl Plants (http://plants.ensembl.org/index.html) website under the following accession numbers: *At3g43110, At5g20790, Bd4g31140, Medtr2g043710, Medtr4g124850, Glyma.09G073050, Glyma.13G113000, Glyma.17G046700, Bd4g31140, GRMZM5G832939, HORVU5Hr1G062450, LOC_Os09g26670, Pavir.2KG347804, Sevir.2G225900, Sobic.002G214300, TRIAE_CS42_5AL_TGACv1_376348_AA1235560, TRIAE_CS42_5BL_TGACv1_407440_AA1356920,* and *TRIAE_CS42_5DL_TGACv1_434454_AA1436290.*

Supplemental data

The following materials are available in the online version of this article.

Supplemental Figure S1. GUS staining assay of the *proAt3g43110::GUS* and *proAt5g20790::GUS* transgenic lines.

Supplemental Figure S2. Tissue-specific expression profiles of *AtRFS1* (At3g43110) and *AtRFS2* (At5g20790).

Supplemental Figure S3. Phylogeny and conservation of RFS proteins in diverse plant species.

Supplemental Figure S4. Expression changes of monocot and dicot *RFS* genes under P-limitation or environmental stimuli.

Supplemental Figure S5. Expression profiles of *ZmRFS* (GRMZM5g832939) and *OsRFS* (LOC_Os09g26670) along a leaf developmental gradient.

Supplemental Figure S6. High magnification micrographs of AtRFS1-GFP transiently expressed in *N. benthamiana* leaf epidermal cells.

Supplemental Figure S7. Senescence phenotypes of *B. distachyon* wild-type (BD21-3), *BdRFS* overexpressors (OX), and CRISPR-ko mutants.

Supplemental Figure S8. Box plots of total chlorophyll content of *B. distachyon* shoot tissue wild-type (BD21-3), *BdRFS* overexpressors (OX), and CRISPR-ko mutants.

Supplemental Figure S9. Molecular characterization of *BdRFS*-targeted CRISPR mutants.

Supplemental Figure S10. Phenotype of 7-day-old *B. distachyon* wild-type (BD21-3) and *crispr*#9 knockout mutant.

Supplemental Figure S11. Phenotype of *B. distachyon* wild-type (BD21-3), *BdRFS* overexpressor (OX) and CRISPR-ko mutant grown under extra-long day (20-h light and 4-h dark) conditions.

Supplemental Figure S12. Expression analysis of *BdFT1* and *BdFT2* genes in the *crispr*#9 mutant.

Supplemental Figure S13. Photochemical analysis of mature *B. distachyon* wild-type (BD21-3) and CRISPR-ko plants.

Supplemental Figure S14. Genotypic and phenotypic characterization of Arabidopsis *RFS* mutants.

Supplemental Figure S15. Acyl group distribution and DBI of total lipids of shoot tissue of CRISPR-ko mutants and overexpressor (OX) lines.

Supplemental Table S1. Physicochemical properties of RFS proteins in plants.

Supplemental Table S2. Prenyl-lipid levels (mg g^{-1} dry weight) of mature leaves in *B. distachyon* wild-type (BD21-3), *BdRFS* CRIPSR-ko mutants and overexpressor (OX) lines.

Supplemental Table S3. Acyl groups distribution of each polar lipid species in BD21-3 and *crispr*#9.

Supplemental Table S4. Acyl groups distribution of each polar lipid species in BD21-3 and OX3.

Supplemental Table S5. Acyl groups distribution of each polar lipid species in Col-0 and *dmu*.

Supplemental Table S6. Summary of BdRFS-interacting protein identified by Co-IP.

Supplemental Table S7. Sequences of primers used in this study.

Acknowledgments

The authors wish to thank colleagues at Noble Research Institute for their help and support: Dr. Miao Chen for pRGEB32 vector construction, Sylvia Warner and Shulan Zhang for lab and greenhouse assistance, and Jianfei Yun and Dr. Qingzhen Jiang for providing *B. distachyon* transformation service. We also thank colleagues at Michigan State University: Drs. Ian Major, Nathan Havko, and Anthony Schilmiller for assistance with phytohormone measurements, Febri Susanto, and Alicia Withrow of the Center for Advance Imaging (MSU) for TEM imaging, Douglas Whitten of the Proteomics Core Facility (MSU) for assistance with LC–MS/MS analysis, and Dr. Christoph Benning and Ron Cook for assistance with TLC and GC analysis.

Funding

This work has been funded by the USDA Umbrella Program (MICL02633) to P.K.L, and by the Noble Research Institute LLC to S.Y. and W.R.S.

Conflict of interest statement. The authors have submitted a provisional patent application with the USPTO related to the results described in this manuscript.

References

Ali U, Lu S, Fadlalla T, Iqbal S, Yue H, Yang B, Hong Y, Wang X, Guo L (2022) The functions of phospholipases and their hydrolysis products in plant growth, development and stress responses. Prog Lipid Res **86**: 101158

Almagro Armenteros JJ, Salvatore M, Emanuelsson O, Winther O, von Heijne G, Elofsson A, Nielsen H (2019) Detecting sequence signals in targeting peptides using deep learning. Life Sci Alliance **2**: e201900429

Bari R, Datt Pant B, Stitt M, Scheible W-R (2006) PHO2, MicroRNA399, and PHR1 define a phosphate-signaling pathway in plants. Plant Physiol **141**: 988–999

Bheemanahalli R, Sathishraj R, Manoharan M, Sumanth HN, Muthurajan R, Ishimaru T, Krishna JSV (2017) Is early morning flowering an effective trait to minimize heat stress damage during flowering in rice? Field Crops Res **203**: 238–242

Bouché F, Woods DP, Linden J, Li W, Mayer KS, Amasino RM, Périlleux C (2022) EARLY FLOWERING 3 and photoperiod sensing in *Brachypodium distachyon*. Front Plant Sci **12**: 769194

Browse J, Roughan PG, Slack CR (1981) Light control of fatty acid synthesis and diurnal fluctuations of fatty acid composition in leaves. Biochem J **196**: 347–354

Bustos R, Castrillo G, Linhares F, Puga MI, Rubio V, Pérez-Pérez J, Solano R, Leyva A, Paz-Ares J (2010) A central regulatory system largely controls transcriptional activation and repression responses to phosphate starvation in Arabidopsis. PLoS Genet **6**: e1001102

Castrillo G, Teixeira P, Paredes S, Law TF, de Lorenzo L, Feltcher ME, Finkel OM, Breakfield NW, Mieczkowski P, Jones CD et al. (2017) Root microbiota drive direct integration of phosphate stress and immunity. Nature **543**: 513–518

Cho LH, Yoon J, An G (2017) The control of flowering time by environmental factors. Plant J **90**: 708–719

Chong L, Xu R, Huang P, Guo P, Zhu M, Du H, Sun X, Ku L, Zhu JK, Zhu Y (2022) The tomato OST1-VOZ1 module regulates drought-mediated flowering. Plant Cell **34**: 2001–2018

Cockram J, Jones H, Leigh FJ, O'Sullivan D, Powell W, Laurie DA, Greenland AJ (2007) Control of flowering time in temperate cereals: genes, domestication, and sustainable productivity. J Exp Bot **58**: 1231–1244

Cook R, Lupette J, Benning C (2021) The role of chloroplast membrane lipid metabolism in plant environmental responses. Cells **10**: 706

Czechowski T, Stitt M, Altmann T, Udvardi MK, Scheible W-R (2005) Genome-wide identification and testing of superior reference genes for transcript normalization in Arabidopsis. Plant Physiol **139**: 5–17

David LC, Girin T, Fleurisson E, Phommabouth E, Mahfoudhi A, Citerne S, Berquin P, Daniel-Vedele F, Krapp A, Ferrario-Méry S (2019) Developmental and physiological responses of *Brachypodium distachyon* to fluctuating nitrogen availability. Sci Rep **9**: 3824–3824

Dhindsa RS, Plumb-Dhindsa P, Thorpe TA (1981) Leaf senescence: correlated with increased levels of membrane permeability and lipid peroxidation, and decreased levels of superoxide dismutase and catalase. J Exp Bot **32**: 93–101

Draper HH, Hadley M (1990) Malondialdehyde determination as index of lipid Peroxidation. Methods in Enzymology, Vol **186**. Academic Press, Cambridge, MA, pp 421–431

Earley KW, Haag JR, Pontes O, Opper K, Juehne T, Song K, Pikaard CS (2006) Gateway-compatible vectors for plant functional genomics and proteomics. Plant J **45**: 616–629

Espinoza-Corral R, Schwenkert S, Lundquist PK (2021) Molecular changes of *Arabidopsis thaliana* plastoglobules facilitate thylakoid membrane remodeling under high light stress. Plant J **106**: 1571–1587

Fisher LHC, Han J, Corke FMK, Akinyemi A, Didion T, Nielsen KK, Doonan JH, Mur LAJ, Bosch M (2016) Linking dynamic phenotyping with metabolite analysis to study natural variation in drought responses of *Brachypodium distachyon*. Front Plant Sci **7**: 1751

Goodstein DM, Shu S, Howson R, Neupane R, Hayes RD, Fazo J, Mitros T, Dirks W, Hellsten U, Putnam N, et al. (2011) Phytozome: a comparative platform for green plant genomics. Nucleic Acids Res **40**: D1178–D1186

Havko NE, Das MR, McClain AM, Kapali G, Sharkey TD, Howe GA (2020) Insect herbivory antagonizes leaf cooling responses to elevated temperature in tomato. Proc Natl Acad Sci USA **117**: 2211–2217

Hilbert DW, Swift DM, Detling JK, Dyer MI (1981) Relative growth rates and the grazing optimization hypothesis. Oecologia **51**: 14–18

Hong SY, Seo PJ, Yang MS, Xiang F, Park CM (2008a) Exploring valid reference genes for gene expression studies in *Brachypodium distachyon* by real-time PCR. BMC Plant Biol **8**: 112–112

Hong Y, Pan X, Welti R, Wang X (2008b) Phospholipase Dα3 is involved in the hyperosmotic response in *Arabidopsis*. Plant Cell **20**: 803–816

Hong Y, Zhao J, Guo L, Kim S-C, Deng X, Wang G, Zhang G, Li M, Wang X (2016) Plant phospholipases D and C and their diverse functions in stress responses. Prog Lipid Res **62**: 55–74

Hong Y, Zheng S, Wang X (2008c) Dual functions of phospholipase Dα1 in plant response to drought. Mol Plant **1**: 262–269

Hooper CM, Castleden IR, Tanz SK, Aryamanesh N, Millar AH (2016) SUBA4: the interactive data analysis centre for Arabidopsis subcellular protein locations. Nucleic Acids Res **45**: D1064–D1074

Horton P, Park KJ, Obayashi T, Fujita N, Harada H, Adams-Collier CJ, Nakai K (2007) WoLF PSORT: protein localization predictor. Nucleic Acids Res **35**: W585–W587

Jin S, Nasim Z, Susila H, Ahn JH (2021) Evolution and functional diversification of FLOWERING LOCUS T/TERMINAL FLOWER 1 family genes in plants. Semin Cell Dev Biol **109**: 20–30

Kakei Y, Mochida K, Sakurai T, Yoshida T, Shinozaki K, Shimada Y (2015) Transcriptome analysis of hormone-induced gene expression in *Brachypodium distachyon*. Sci Rep **5**: 14476

Kant S, Peng M, Rothstein SJ (2011) Genetic regulation by NLA and MicroRNA827 for maintaining nitrate-dependent phosphate homeostasis in Arabidopsis. PLoS Genetics **7**: e1002021

Karimi M, Inzé D, Depicker A (2002) GATEWAY^{TM} vectors for Agrobacterium-mediated plant transformation. Trends Plant Sci **7**: 193–195

Kazan K, Lyons R (2015) The link between flowering time and stress tolerance. J Exp Bot **67**: 47–60

Kim SJ, Zemelis-Durfee S, Wilkerson C, Brandizzi F (2017) In Brachypodium a complex signaling is actuated to protect cells from proteotoxic stress and facilitate seed filling. Planta **246**: 75–89

Kleinboelting N, Huep G, Kloetgen A, Viehoever P, Weisshaar B (2012) GABI-Kat SimpleSearch: new features of the *Arabidopsis thaliana* T-DNA mutant database. Nucleic Acids Res **40**: D1211–1215

Koda S, Onda Y, Matsui H, Takahagi K, Uehara-Yamaguchi Y, Shimizu M, Inoue K, Yoshida T, Sakurai T, Honda H, et al. (2017) Diurnal transcriptome and gene network represented through sparse modeling in *Brachypodium distachyon*. Front Plant Sci **8**: 2055

Kong XM, Zhou Q, Zhou X, Wei BD, Ji SJ (2019) Transcription factor CaNAC1 regulates low-temperature-induced phospholipid degradation in green bell pepper. J Exp Bot **71**: 1078–1091

Kouzai Y, Kimura M, Yamanaka Y, Watanabe M, Matsui H, Yamamoto M, Ichinose Y, Toyoda K, Onda Y, Mochida K, et al. (2016) Expression profiling of marker genes responsive to the defence-associated phytohormones salicylic acid, jasmonic acid and ethylene in *Brachypodium distachyon*. BMC Plant Biol **16**: 59

Kumar S, Stecher G, Li M, Knyaz C, Tamura K (2018) MEGA X: molecular evolutionary genetics analysis across computing platforms. Mol Biol Evol **35**: 1547–1549

Lambers H, Cawthray GR, Giavalisco P, Kuo J, Laliberté E, Pearse SJ, Scheible W-R, Stitt M, Teste F, Turner BL (2012) Proteaceae from severely phosphorus-impoverished soils extensively replace phospholipids with galactolipids and sulfolipids during leaf development to achieve a high photosynthetic phosphorus-use-efficiency. New Phytol **196**: 1098–1108

Letunic I, Bork P (2021) Interactive Tree Of Life (iTOL) v5: an online tool for phylogenetic tree display and annotation. Nucleic Acids Res **49**: W293–W296

Li HM, Yu CW (2018) Chloroplast galactolipids: the link between photosynthesis, chloroplast shape, jasmonates, phosphate starvation and freezing tolerance. Plant Cell Physiol **59**: 1128–1134

Li M, Welti R, Wang X (2006) Quantitative profiling of Arabidopsis polar glycerolipids in response to phosphorus starvation. Roles of phospholipases D zeta1 and D zeta2 in phosphatidylcholine hydrolysis and digalactosyldiacylglycerol accumulation in phosphorus-starved plants. Plant Physiol **142**: 750–761

Li X (2011) Infiltration of *Nicotiana benthamiana* protocol for transient expression via agrobacterium. Bio-protocol **1**: e95

Lin YL, Tsay YF (2017) Influence of differing nitrate and nitrogen availability on flowering control in Arabidopsis. J Exp Bot **68**: 2603–2609

Liu H, Ding Y, Zhou Y, Jin W, Xie K, Chen LL (2017) CRISPR-P 2.0: an improved CRISPR-Cas9 tool for genome editing in plants. Mol Plant **10**: 530–532

Liu X, Ma D, Zhang Z, Wang S, Du S, Deng X, Yin L (2019) Plant lipid remodeling in response to abiotic stresses. Environ Exp Bot **165**: 174–184

Lundquist PK, Poliakov A, Giacomelli L, Friso G, Appel M, McQuinn RP, Krasnoff SB, Rowland E, Ponnala L, Sun Q, et al. (2013) Loss of plastoglobule kinases ABC1K1 and ABC1K3 causes conditional degreening, modified prenyl-lipids, and recruitment of the jasmonic acid pathway. Plant Cell **25**: 1818–1839

Lv B, Nitcher R, Han X, Wang S, Ni F, Li K, Pearce S, Wu J, Dubcovsky J, Fu D (2014) Characterization of FLOWERING LOCUS T1 (FT1) gene in brachypodium and wheat. PLoS One **9**: e94171

Mann DG, Lafayette PR, Abercrombie LL, King ZR, Mazarei M, Halter MC, Poovaiah CR, Baxter H, Shen H, Dixon RA, et al. (2012) Gateway-compatible vectors for high-throughput gene functional analysis in switchgrass (*Panicum virgatum* L.) and other monocot species. Plant Biotechnol J **10**: 226–236

Mitra SK, Walters BT, Clouse SD, Goshe MB (2009) An efficient organic solvent based extraction method for the proteomic analysis of Arabidopsis plasma membranes. J Proteome Res **8**: 2752–2767

Nakamura Y (2013) Phosphate starvation and membrane lipid remodeling in seed plants. Prog Lipid Res **52**: 43–50

Nakamura Y (2018) Membrane lipid oscillation: an emerging system of molecular dynamics in the plant membrane. Plant Cell Physiol **59**: 441–447

Nakamura Y, Andrés F, Kanehara K, Liu Y-c, Dörmann P, Coupland G (2014) Arabidopsis florigen FT binds to diurnally oscillating phospholipids that accelerate flowering. Nat Commun **5**: 3553

Naumann C, Müller J, Sakhonwasee S, Wieghaus A, Hause G, Heisters M, Bürstenbinder K, Abel S (2019) The local phosphate deficiency response activates endoplasmic reticulum stress-dependent autophagy. Plant Physiol **179**: 460–476

Nilsson L, Muller R, Nielsen TH (2007) Increased expression of the MYB-related transcription factor, PHR1, leads to enhanced phosphate uptake in *Arabidopsis thaliana*. Plant Cell Environ **30**: 1499–1512

Pant BD, Burgos A, Pant P, Cuadros-Inostroza A, Willmitzer L, Scheible W-R (2015) The transcription factor PHR1 regulates lipid remodeling and triacylglycerol accumulation in *Arabidopsis thaliana* during phosphorus starvation. J Exp Bot **66**: 1907–1918

Pfaff J, Denton AK, Usadel B, Pfaff C (2020) Phosphate starvation causes different stress responses in the lipid metabolism of tomato leaves and roots. Biochim Biophys Acta Mol Cell Biol Lipids **1865**: 158763

Priest HD, Fox SE, Rowley ER, Murray JR, Michael TP, Mockler TC (2014) Analysis of global gene expression in *Brachypodium distachyon* reveals extensive network plasticity in response to abiotic stress. PLoS One **9**: e87499–e87499

Qin Z, Bai Y, Muhammad S, Wu X, Deng P, Wu J, An H, Wu L (2019) Divergent roles of FT-like 9 in flowering transition under different day lengths in *Brachypodium distachyon*. Nat Commun **10**: 812

Qin Z, Wu J, Geng S, Feng N, Chen F, Kong X, Song G, Chen K, Li A, Mao L, et al. (2017) Regulation of FT splicing by an endogenous cue in temperate grasses. Nat Commun **8**: 14320–14320

Qiu D, Hu W, Zhou Y, Xiao J, Hu R, Wei Q, Zhang Y, Feng J, Sun F, Sun J, Yang G, He G (2021) TaASR1-D confers abiotic stress resistance by affecting ROS accumulation and ABA signalling in transgenic wheat. Plant Biotechnol J **19**: 1588–1601

Qu L, Chu YJ, Lin WH, Xue HW (2021) A secretory phospholipase D hydrolyzes phosphatidylcholine to suppress rice heading time. PLoS Genet **17**: e1009905

Raissig MT, Woods DP (2022) Chapter Two - The wild grass *Brachypodium distachyon* as a developmental model system. *In* B Goldstein, M Srivastava, eds, Current Topics in Developmental Biology, Vol **147**. Academic Press, Cambridge, MA, pp 33–71

Raza A, Charagh S, Zahid Z, Mubarik MS, Javed R, Siddiqui MH, Hasanuzzaman M (2021) Jasmonic acid: a key frontier in conferring abiotic stress tolerance in plants. Plant Cell Rep **40**: 1513–1541

Ream TS, Woods DP, Schwartz CJ, Sanabria CP, Mahoy JA, Walters EM, Kaeppler HF, Amasino RM (2013) Interaction of photoperiod and vernalization determines flowering time of *Brachypodium distachyon* Plant Physiol **164**: 694–709

Riboni M, Galbiati M, Tonelli C, Conti L (2013) GIGANTEA enables drought escape response via abscisic acid-dependent activation of the florigens and SUPPRESSOR OF OVEREXPRESSION OF CONSTANS1 Plant Physiol **162**: 1706–1719

Rubio V, Linhares F, Solano R, Martín AC, Iglesias J, Leyva A, Paz-Ares J (2001) A conserved MYB transcription factor involved in phosphate starvation signaling both in vascular plants and in unicellular algae. Genes Dev **15**: 2122–2133

Sang Y, Zheng S, Li W, Huang B, Wang X (2001) Regulation of plant water loss by manipulating the expression of phospholipase Dα. Plant J **28**: 135–144

Scholthof KBG, Irigoyen S, Catalan P, Mandadi KK (2018) Brachypodium: a monocot grass model genus for plant biology. Plant Cell **30**: 1673–1694

Schwartz CJ, Doyle MR, Manzaneda AJ, Rey PJ, Mitchell-Olds T, Amasino RM (2010) Natural variation of flowering time and vernalization responsiveness in *Brachypodium distachyon*. BioEnergy Res **3**: 38–46

Shavrukov Y, Kurishbayev A, Jatayev S, Shvidchenko V, Zotova L, Koekemoer F, de Groot S, Soole K, Langridge P (2017) Early flowering as a drought escape mechanism in plants: how can it aid wheat production? Front Plant Sci **8**: 1950

Shaw LM, Lyu B, Turner R, Li C, Chen F, Han X, Fu D, Dubcovsky J (2019) FLOWERING LOCUS T2 regulates spike development and fertility in temperate cereals. J Exp Bot **70**: 193–204

Shevchenko A, Wilm M, Vorm O, Mann M (1996) Mass spectrometric sequencing of proteins silver-stained polyacrylamide gels. Anal Chem **68**: 850–858

Sun Q, Zybailov B, Majeran W, Friso G, Olinares PD, van Wijk KJ (2009) PPDB, the plant proteomics database at cornell. Nucleic Acids Res **37**: D969–D974

Sun Y, Jain A, Xue Y, Wang X, Zhao G, Liu L, Hu Z, Hu S, Shen X, Liu X, et al. (2020) OsSQD1 at the crossroads of phosphate and sulfur metabolism affects plant morphology and lipid composition in response to phosphate deprivation. Plant Cell Environ **43**: 1669–1690

Susila H, Jurić S, Liu L, Gawarecka K, Chung KS, Jin S, Kim SJ, Nasim Z, Youn G, Suh MC, et al. (2021) Florigen sequestration in cellular membranes modulates temperature-responsive flowering. Science **373**: 1137–1142

Takáč T, Pechan T, Šamajová O, Šamaj J (2019) Proteomic analysis of Arabidopsis pldα1 mutants revealed an important role of phospholipase D alpha 1 in chloroplast biogenesis. Front Plant Sci **10**: 89

van Wijk KJ, Kessler F (2017) Plastoglobuli: plastid microcompartments with integrated functions in metabolism, plastid developmental transitions, and environmental adaptation. Ann Rev Plant Biol **68**: 253–289

Vigh L, Huitema H, Woltjes J, van Hasselt PR (1986) Drought stress-induced changes in the composition and physical state of phospholipids in wheat. Physiol Plant **67**: 92–96

Wang L, Hu W, Feng J, Yang X, Huang Q, Xiao J, Liu Y, Yang G, He G (2016) Identification of the ASR gene family from *Brachypodium distachyon* and functional characterization of BdASR1 in response to drought stress. Plant Cell Rep **35**: 1221–1234

Wang X (2005) Regulatory functions of phospholipase D and phosphatidic acid in plant growth, development, and stress responses. Plant Physiol **139**: 566–573

Wang X, Guo L, Wang G, Li M (2014) PLD: phospholipase Ds in plant signaling. In X Wang, ed, Phospholipases in Plant Signaling. Springer Berlin Heidelberg, Berlin, Heidelberg, Germany, pp 3–26

Wang Z, Benning C (2011) *Arabidopsis thaliana* polar glycerolipid profiling by Thin Layer Chromatography (TLC) coupled with Gas-Liquid Chromatography (GLC). J Vis Exp **18**: 2518

Wasternack C, Song S (2016) Jasmonates: biosynthesis, metabolism, and signaling by proteins activating and repressing transcription. J Exp Bot **68**: 1303–1321

Welti R, Li W, Li M, Sang Y, Biesiada H, Zhou HE, Rajashekar CB, Williams TD, Wang X (2002) Profiling membrane lipids in plant stress responses: role of phospholipase dα in freezing-induced lipid changes in Arabidopsis. J Biol Chem **277**: 31994–32002

Woods D, Dong Y, Bouche F, Bednarek R, Rowe M, Ream T, Amasino R (2019) A florigen paralog is required for short-day vernalization in a pooid grass. eLife **8**: e42153

Woods DP, Bednarek R, Bouché F, Gordon SP, Vogel JP, Garvin DF, Amasino RM (2017) Genetic Architecture of Flowering-Time Variation in *Brachypodium distachyon*. Plant Physiol **173**: 269–279

Wu L, Liu D, Wu J, Zhang R, Qin Z, Liu D, Li A, Fu D, Zhai W, Mao L (2013) Regulation of FLOWERING LOCUS T by a MicroRNA in *Brachypodium distachyon*. Plant Cell **25**: 4363–4377

Xie K, Minkenberg B, Yang Y (2015) Boosting CRISPR/Cas9 multiplex editing capability with the endogenous tRNA-processing system. Proc Natl Acad Sci USA **112**: 3570–3575

Yang Y, Zienkiewicz A, Lavell A, Benning C (2017) Coevolution of domain interactions in the chloroplast TGD1, 2, 3 lipid transfer complex specific to Brassicaceae and Poaceae plants. Plant Cell **29**: 1500–1515

Ying S, Blancaflor EB, Liao F, Scheible W-R (2022) A phosphorus-limitation induced, functionally conserved DUF506 protein is a repressor of root hair elongation in plants. New Phytologist **233**: 1153–1171

Yoon JS, Kim JY, Kim DY, Seo YW (2021) A novel wheat ASR gene, TaASR2D, enhances drought tolerance in *Brachypodium distachyon*. Plant Physiol Biochem **159**: 400–414

Yoon JS, Kim JY, Lee MB, Seo YW (2019) Over-expression of the Brachypodium ASR gene, BdASR4, enhances drought tolerance in *Brachypodium distachyon*. Plant Cell Rep **38**: 1109–1125

Yu L, Zhou C, Fan J, Shanklin J, Xu C (2021) Mechanisms and functions of membrane lipid remodeling in plants. Plant J **107**: 37–53